

1 **Using flow cytometry and light-induced fluorescence technique to characterize the**
2 **variability and characteristics of bioaerosols in springtime at Metro Atlanta, Georgia**

3
4 Arnaldo Negron^{a,b}, Natasha DeLeon-Rodriguez^{c§}, Samantha M. Waters^{a#}, Luke D. Ziemba^d,
5 Bruce Anderson^d, Michael Bergin^e, Konstantinos T. Konstantinidis^{f,c*}, and Athanasios Nenes^{a,g,h*}

6 ^a School of Earth and Atmospheric Sciences, Georgia Institute of Technology, Atlanta, GA 30332, USA

7 ^b School of Chemical and Biomolecular Engineering, Georgia Institute of Technology, Atlanta, GA
8 30332, USA

9 ^c School of Biology, Georgia Institute of Technology, Atlanta, GA 30332, USA

10 ^d Chemistry and Dynamics Branch/Science Directorate, National Aeronautics and Space Administration
11 Langley Research Center, Hampton, VA 23681, USA

12 ^e Department of Civil and Environmental Engineering, Duke University, Durham, NC, 2770, USA

13 ^f School of Civil and Environmental Engineering, Georgia Institute of Technology, Atlanta, GA 30332,
14 USA

15 ^g Institute for Chemical Engineering Science, Foundation for Research and Technology Hellas, Patra,
16 GR-26504, Greece

17 ^h Laboratory of Atmospheric Processes and their Impacts (LAPI), School of Architecture, Civil &
18 Environmental Engineering, Ecole Polytechnique Fédérale de Lausanne, CH-1015, Switzerland

19 [§] Currently at: Puerto Rico Science, Technology and Research Trust, Rio Piedras, 00927, Puerto Rico

20 [#] Currently at: Department of Marine Sciences, University of Georgia, Athens, GA 30602-3636

21 ^{*}Corresponding Author

22 **Abstract**

23 The abundance and speciation of primary biological aerosol particles (PBAP) is important for
24 understanding their impacts on human health, cloud formation and ecosystems. Towards this, we have
25 developed a protocol for quantifying PBAP collected from large volumes of air with a portable wet-walled
26 cyclone bioaerosol sampler. A flow cytometry (FCM) protocol was then developed to quantify and
27 characterize the PBAP populations from the sampler, which were confirmed against epifluorescence
28 microscopy. The sampling system and FCM analysis were used to study PBAP in Atlanta, GA over a two-
29 month period and showed clearly defined populations of DNA-containing particles: Low Nucleic Acid-
30 content particles above threshold (LNA-AT), and High Nucleic Acid-content particles (HNA) likely
31 containing wet-ejected fungal spores and pollen. We find that daily-average springtime PBAP concentration
32 (1 to 5 μ m diameter) ranged between 1.4×10^4 and 1.1×10^5 m⁻³. The LNA-AT population dominated PBAP
33 during dry days ($72 \pm 18\%$); HNA dominated the PBAP during humid days and following rain events,
34 where HNA comprised up to 92% of the PBAP number. Concurrent measurements with a Wideband
35 Integrated Bioaerosol Sensor (WIBS-4A) showed that FBAP and total FCM counts are similar; HNA (from

36 FCM) moderately correlated with ABC type FBAP concentrations throughout the sampling period (and for
37 the same particle size range, 1-5 μm diameter). However, the FCM LNA-AT population, possibly
38 containing bacterial cells, did not correlate with any FBAP type. The lack of correlation of any WIBS FBAP
39 type with the LNA-AT suggest airborne bacterial cells may be more difficult to unambiguously detect with
40 autofluorescence than currently thought. Identification of bacterial cells even in the FCM (LNA-AT
41 population) is challenging, given that the fluorescence level of stained cells at times may be comparable to
42 that seen from abiotic particles. HNA and ABC displayed highest concentration on a humid and warm day
43 after a rain event (4/14), suggesting that both populations correspond to wet-ejected fungal spores. Overall,
44 information from both instruments combined reveals a highly dynamic airborne bioaerosol community over
45 Atlanta, with a considerable presence of fungal spores during humid days, and LNA-AT population
46 dominating bioaerosol community during dry days.

47 **Introduction**

48 Primary biological aerosol particles (PBAP), also called bioaerosols, are comprised of airborne
49 microbial cells (e.g. bacteria, diatoms), reproductive entities (e.g. pollen, fungal spores), viruses and
50 biological fragments. Bioaerosols are ubiquitous, with potentially important impacts on human health,
51 cloud formation, precipitation, and biogeochemical cycles. (Pöschl, 2005; Hoose et al., 2010; DeLeon-
52 Rodriguez et al., 2013; Morris et al., 2014; Longo et al., 2014; Fröhlich-Nowoisky et al., 2016;
53 Myriokefalitakis et al., 2016). Despite their low number concentration relative to abiotic particles, PBAP
54 possess unique functional and compositional characteristics that differentiate them from abiotic aerosol.
55 For example, certain PBAP constitute the most efficient of atmospheric ice nucleators, affecting the
56 microphysics of mixed phase clouds and precipitation (Hoose and Möhler, 2012; Sullivan et al., 2017). The
57 mass and nutrient content of PBAP may suffice to comprise an important supply of bioavailable P to
58 oligotrophic marine ecosystems (Longo et al., 2014; Myriokefalitakis et al., 2016). In addition, the
59 concurrence of disease outbreaks during dust storms has been attributed to pathogenic microbes attached
60 to airborne dust that are subsequently inhaled (Griffin et al., 2003; Ortiz-Martinez et al., 2015; Goudie
61 2014).

62 Quantification of the concentration and size of PBAP is critical for understanding their environmental
63 impacts. Measuring PBAP however poses a challenge for established microbiology tools, owing to their
64 low atmospheric concentration ($10^3 - 10^6$ cells m^{-3} air; Fröhlich-Nowoisky et al., 2016) and wide diversity
65 of airborne particle types and sizes. For instance, only a fraction of microorganisms (an estimated 5%; Chi
66 and Li et al., 2007) can be cultured, and cultivation cannot be used to quantify dead organisms, viruses or
67 fragments, while most culture-independent methods are optimized for more abundant microbial
68 populations. Epifluorescence microscopy (EPM) is the standard for bioaerosol quantification but is not

69 high-throughput and requires considerable time for quantification of concentration per sample. Flow
70 cytometry (FCM) is an analysis technique based on the concurrent measurement of light scattering and
71 fluorescence intensity from single particles (Wang et al., 2010). FCM requires a liquid suspension of
72 bioparticles that flows through an optical cell and interrogated with a series of laser beams. Each sample is
73 pretreated with stains that targeting specific macromolecules (e.g. DNA/RNA) which subsequently
74 fluoresce when excited by the FCM lasers. The resulting scattering and fluorescent light emissions are then
75 detected by an array of sensors to allow the differentiation of biological and abiotic (e.g. dust) particles
76 according to the characteristic specific to the stain used. FCM has proved to be as reliable as EPM, but with
77 the advantage of lower uncertainty, higher quantification efficiency and requiring considerably less time
78 and effort than EPM per sample (Lange et al., 1997). FCM is frequently used in biomedical research to
79 quantify eukaryotic cell populations, and in microbiology to quantify a wide variety of yeast and bacterial
80 cells (Nir et al., 1990; Van Dilla et al., 1983). FCM is also used to study environmental samples, e.g., to
81 differentiate low nucleic acid (LNA) from high nucleic acid (HNA) phytoplankton in aquatic environments
82 (Wang Y. et al 2010; Müller et al., 2010). Despite its advantages, FCM has seen little use in the bioaerosol
83 field to date (e.g., Chen and Li, 2005; Liang et al., 2013), owing in part to the challenges associated with
84 collecting sufficient PBAP mass for robust counting statistics to be obtained (Chen and Li, 2005; Liang et
85 al., 2013). Chen and Li (2005) determined that for counting purposes, the SYTO-13 nucleic acid stain is
86 the most effective (among five different nucleic acid stains studied) for determining reliable concentration
87 of bioaerosols. SYTO-13 stain can also be used to provide insights on the stress/metabolic state of microbes.
88 Guindulian et al. (1997), with starved seawater samples and *E.coli* pure cultures together suggest that the
89 stress level caused by marine starvation reduces RNA content in aquatic microorganisms to an undetectable
90 level. This has important implications for the detection of atmospheric PBAP, as cells are exposed to
91 multiple stressors when airborne.

92 Light Induced Fluorescence (LIF) is an increasingly utilized technique for bioaerosol quantification,
93 and it relies on measuring the autofluorescence intensity of specific high yield fluorophores (e.g.,
94 Nicotinamide Adenine Dinucleotide – NADH co-enzyme, flavins and amino acids like Tryptophan and
95 Tyrosine) present in PBAP. The major advantage of the technique is that it is fully automated, does not
96 require a liquid suspension (i.e., it directly senses particles suspended in air) and it provides high frequency
97 measurements (~1 Hz) make it ideal for monitoring and operation in highly variable environments (e.g.,
98 aircraft operation). Particles detected by LIF, called Fluorescent Biological Aerosol Particles (FBAP),
99 although not equal to PBAP, may still constitute a large fraction of the biological particles (Healy et al.,
100 2014; Gosselin et al., 2016). Using LIF, FBAP diurnal cycles showing maximum concentrations during
101 evenings and minimum around middays, especially in heavily vegetated environments have been observed.
102 This behavior has been related to known temperature and relative humidity release mechanism of certain

103 fungal spore species (Wu et al., 2007; Gabey et al., 2010; Tropak and Schnaiter, 2013). Huffman et al.
104 (2010) used a UV-Aerodynamic Particle Sizer (UV-APS) to show that the concentration and frequency of
105 occurrence of 3 μ m FBAP particles at Mainz, Germany (semi-urban environment) exhibited a strong diurnal
106 cycle from August through November: with a first peak at $\sim 1.6 \times 10^4 \text{ m}^{-3}$ at mid-morning (6-8 am) followed
107 by a constant profile ($\sim 2\text{-}4 \times 10^4 \text{ m}^{-3}$) throughout the rest of the day. Similar studies in urban and densely
108 vegetated environments suggest a notable difference in the size distributions, diurnal behavior and FBAP
109 loading between the two environments. Gabey et al., 2011 found that the FBAP in Manchester, UK follow
110 a characteristic bimodal distribution with peaks at 1.2 μ m and 1.5 – 3.0 μ m. As in Mainz, the concentration
111 of larger particles peaks in the mid-morning, ranges from 0 to 300 L^{-1} , and the 1.2 μ m peak is linked to
112 traffic activity. However, at the Borneo tropical rain forest FBAP concentrations peak during the evening
113 with a robust 2-3 μ m population and concentrations ranging from 100 to 2000 L^{-1} (Gabey et al., 2010).

114 LIF-based observations (e.g. UV-APS, WIBS), combined with measurements of molecular tracers (e.g.
115 mannitol and arabitol) and endotoxin measurements provide a more complete picture of PBAP emissions.
116 Gosselin et al. (2016) applied this approach during the BEACHON-RoMBAS field campaign. A clear
117 correlation between FBAP and the molecular markers is seen, indicating an increase of fungal spores during
118 rain events. FBAP concentrations and molecular marker-inferred (arabitol and mannitol) fungal spore
119 concentrations (1.7pg mannitol per spore and 1.2 pg arabitol per spore; Bauer et al., 2008) were within the
120 same order of magnitude. The UV-APS FBAP concentration during rain events was higher than the fungal
121 spore concentrations inferred from the concentration of molecular markers, which suggest other non-fungal
122 spore fluorescent particles are detected as well as fungal spores by the UV-APS. In the same study, the
123 WIBS-3 cluster (determined using Crawford et al., 2015) linked to fungal spores gave concentrations that
124 were 13% lower than those derived from molecular marker concentrations during rain events. During dry
125 events, FBAP and molecular markers derived fungal spore concentrations were poorly correlated. It is
126 currently unknown the degree to which all types of PBAP are consistently detected by LIF over different
127 time of the year and different environments; it is likely, however, that for certain classes of bioparticles
128 (e.g., pollen and fungi) the detection efficiency using LIF is relatively high. However, the low intrinsic
129 fluorescence intensity of bacteria and high variability of thereof in relation to metabolic state may lead to
130 their misclassification as non-biological particles (Hernandez et al., 2016).

131 For LIF-based quantification of PBAP to be effective, it requires the intrinsic fluorescence of biological
132 material to exceed that of non-biological matter. Depending on the type, metabolic state and species, PBAP
133 autofluorescence may vary orders of magnitude and therefore LIF may not always be able to differentiate
134 between biological and abiotic particles. For example, Tropak and Schnaiter (2013) showed that laboratory-
135 generated mineral dust, soot and ammonium sulfate may be misclassified as FBAP. To address

136 misclassification, Excitation Emission Matrices (EEMs) have been developed for biomolecules (e.g.
137 tryptophan, tyrosine, riboflavin) and non-biological (e.g. Pyrene, Naphthalene, Humic Acid) molecules.
138 EEMs provide the wavelength-dependent fluorescence emission spectra as a function of the excitation
139 wavelength and are used to assign spectral modes to known fluorophores. The structure of EEMs is
140 important for identifying molecules that are unique to PBAP and allow their identification by LIF; it is this
141 principle upon which detectors in commercial FBAP measurements (e.g. WIBS, UV-APS) are based upon.
142 Comparison of EEMs from biological and non-biological molecules show that even when biomolecules
143 have higher autofluorescence intensity than non-biologicals in the LIF detection range, interferences from
144 non-biological compounds (e.g. polycyclic aromatic hydrocarbons and soot) from combustion emissions
145 can influence LIF detection (Pöhlker et al., 2012). Considerable work remains on determining which
146 detector(s) or combination thereof provides an unambiguous identification of bioaerosols and related
147 subgroups (e.g. bacteria, fungal spores, pollen). Towards this, an aerobiology catalog of pure cultures has
148 been developed for the WIBS-4 (Hernandez et al., 2016), where, (i) pollen and fungal spore species
149 autofluoresce much more than bacteria, and, (ii) bioaerosol subgroups are more successfully discriminated
150 by specific detector(s). However, the same study showed that instrument-to-instrument variability in
151 fluorescence detection poses a considerable challenge, as applying common detection thresholds across
152 instruments leads to considerable differences in PBAP concentration and composition.

153 Another important issue for LIF-based PBAP is the impact of atmospheric oxidants, UV and other
154 stressors on the fluorescence intensity of PBAP. This is important, given the ubiquity of PBAP throughout
155 the atmosphere, including the extreme conditions in the upper troposphere (DeLeon-Rodriguez et al., 2013).
156 Pan et al. (2014) tested the effect of relative humidity and ozone exposure in the autofluorescence spectra
157 of octapeptide aerosol particles using an UV-APS connected to a rotating drum. Octapeptides, organic
158 molecules containing eight amino acids and present in cells, were used as a proxy to study the aging of
159 tryptophan and results suggest bioaerosols exposure to typical ozone concentrations (~150ppb) decrease
160 tryptophan fluorescence intensity and affects PBAP detection. Laboratory experiments cannot always
161 reproduce the wide variety of environmental conditions and stressors that can affect the metabolism state
162 of microbes, and hence their autofluorescence. Joly et al. (2015) studied the survival rate of multiple
163 bacterial (e.g. *Pseudomonas syringae*, *Sphingomonas sp.* And *Arthrobacter sp.*) and yeast (e.g. *Dioszegia*
164 *hungarica*) strains isolated from cloud water upon exposure to oxidants (e.g. H₂O₂), solar light (e.g. UV
165 radiation), osmotic shocks (e.g. multiple NaCl concentrations) and freeze-thaw cycles. Among these
166 stressors, the freeze-thaw cycles affected most the survival rate (quantified as the quotient of the colony
167 forming unit (CFU) counts before and after exposure to each stressor dose) of bacterial cells. *Arthrobacter*
168 *sp.* showed the lowest survival rates (< 20%) per cycle, and the highest survival rate of all bacterial strains
169 was observed at 10⁸ cell mL⁻¹ (highest concentration), suggesting that high cell concentrations lead to cell

170 aggregation and provided protection against freeze-thaw cycles. The survival rate of the yeast *Dioszegia*
171 *hungarica* was mostly affected by UV radiation showing the effect of each stressor in the survival rate of
172 cells may depend on the characteristics of each cell. Even though the survival rate and the intrinsic
173 fluorescence intensity of bioaerosols have not been correlated, multiple stressors can be affecting
174 bioaerosols LIF detection and these issues regarding the use of LIF need to be resolved to fully understand
175 their PBAP detection efficiency over the wide range of atmospheric conditions and PBAP population
176 composition (Toprak and Schnaiter, 2013; Hernandez et al., 2016).

177 The aims of the study were to (i) develop an effective and reliable FCM detection and quantification
178 protocol for bioaerosol; (ii) apply the protocol to understand bioaerosol populations and their variability
179 during different meteorological conditions, and, (iii) compare FCM and WBS-4A results to have a better
180 understanding of PBAP day-to-day variability. To our knowledge, this study is the first to develop a FCM
181 protocol to identify and quantify well-defined speciated bioaerosols populations from samples collected
182 from a modified state-of-the-art biosampler. LIF sampling of bioaerosol side-by-side with established and
183 quantitative biology tools (FCM and EPM) was conducted to assess the LIF detection capabilities toward
184 different bioaerosol populations and under atmospherically-relevant conditions during this study. Atlanta
185 is selected as a case study for PBAP sampling, as it provides a highly populated urban environment
186 surrounded by vast vegetative areas; this and the broad range of temperature and humidity ensures a wide
187 range of PBAP population composition, state and concentrations. All the samples collected are compared
188 side-by-side to concurrent WBS-4A data collected over the same time period.

189 **2. Instrumentation and Methodology**

190 **2.1 Bioaerosol Sampler**

191 Sampling was performed using the SpinCon II (InnovaPrep LLC, Inc.) portable wet-walled cyclone
192 aerosol sampler. Aerosol is collected by inertial impaction with a recirculating liquid film in the cyclone;
193 evaporative losses are compensated so that the sample volume is maintained constant during a sample cycle.
194 The particle collection efficiency for 1 μ m, 3 μ m, 3.5 μ m and 5.0 μ m particles is about 47.3 \pm 2.1%,
195 56.1 \pm 3.9%, 14.6 \pm 0.6 and 13.8 \pm 2.2%, respectively (Kesavan et al., 2015). However, the experiments
196 conducted using 1 μ m PSL and 3 μ m PSL, 3.5 μ m oleic acid and 5.0 μ m oleic acid particles not necessarily
197 quantify the collection efficiency of biological particles in this size range. Even with a lower efficiency
198 than any impingement sampler, SpinCon has a better performance (product of the flow rate and the
199 sampling efficiency) than any impingement sampler due to its high volumetric flow rate, which make it
200 more suitable for bioaerosols detection (Kesavan et al., 2015). The efficiency, power consumption and
201 performance of 29 biosamplers were analyzed by Kesavan et al. (2015) to determine which are best suited
202 for indoor or outdoor sampling. The study concluded biosamplers effectiveness will be determined by their

203 performance in the size range of interest, rather than just by looking its sampling efficiency. Furthermore,
204 Santl-Temkiv et al. (2017) recently studied SpinCon retention efficiency towards sea water heterogenous
205 and pure cultured *P.agglomerans* populations ($\sim 10^5$ cells mL⁻¹) after 1 hr sampling period by comparing
206 FCM-derived concentrations (using SYBR green stain) before and after the sampling period. SpinCon
207 retains $20.6\pm 5.8\%$ of the *P.agglomerans* concentration, whereas $55.3\pm 2.1\%$ of the sea water microbial
208 concentration is retained after sampling for 1h

209 In our study, the biosampler was run at 478L min^{-1} for 4hr sampling cycles. Phosphate-buffered saline
210 (PBS) 1X pH 7.4 solution was used and the instrument compensated evaporation by supplying Milli-Q
211 water to maintain the PBS concentration constant. Upon termination of each sampling cycle, the instrument
212 was programmed to dispense the sample in a 15mL centrifuge tube. Then, 10 μ l of formalin (37 wt.%
213 formaldehyde) per mL of solution was added to every sample for preservation and samples were stored at
214 4°C. Given the long sampling times and the low concentration of PBAP, the fluid supply system of the
215 instrument was modified and a cleaning protocol (CP) has been developed, which is described below.

216 SpinCon II water and PBS supply bags were replaced by two 2L autoclavable Nalgene bottles (Thermo
217 Scientific Inc.) with antimicrobial tubing, connectors and a small HEPA filter connected to vent and prevent
218 coarse and submicron particles contamination (Figure 1). Bottles were autoclaved and filled with Milli-Q
219 water and PBS, beforehand sterilized with 0.2 μ m pore bottle top filters (Thermo Fisher Inc.) and transferred
220 inside a biosafety cabinet. An aliquot of each fluid obtained after preparation was evaluated for sterility by
221 EPM and FCM.

222 The cleaning protocol (CP) of the biosampling system consists of two phases. During phase one, all
223 acrylic windows and the outside of the collector/concentrator were cleaned with ethanol 70 wt. %. Then,
224 the instrument inlet, outlet, and the inside of the collector/concentrator was cleaned with ethanol 70 wt. %.
225 In the second phase, the SpinCon II inlet was connected to a HEPA filter to provide a particle-free source
226 of air to the sampling system; the instrument was then washed with ethanol 70 wt.%, 10 wt.% bleach
227 solution, PBS and Milli-Q H₂O, respectively. The wash consisted of a rinse, a 2 minutes sample and filling
228 the instrument collector/concentrator with the fluid in use (i.e., bleach solution, ethanol, PBS and Milli-Q
229 H₂O). The collector/concentrator was drained after 1 minute. The above were repeated for the remaining
230 fluids, taking 5 minutes per fluid. Overall, the CP requires 45 minutes; upon completion, a blank is obtained
231 to constrain the residual contamination levels after cleaning (described below). Finally, the HEPA filter
232 was disconnected, instrument inlets and outlets were sealed and the inlet tube was cleaned with ethanol 70
233 wt.% to be ready for rooftop sampling. SpinCon II was rinsed with ethanol 70wt.% after each sampling
234 episode and the cleaning protocol was applied before each sample.

235 Several blanks were obtained to quantify the levels of PBAP contamination in the fluids and sampler,
236 and to ensure that they were sufficiently low to not bias the detection, identification and quantification of
237 the PBAP. Furthermore, an instrument blank was obtained after a CP to constrain residual particles, by
238 running the sampler for 2 minutes, while sampling air with a HEPA filter connected to the inlet of the
239 SpinCon II. Another blank was collected to characterize any contamination of biological particles from the
240 supply of PBS and water in the SpinCon II. This was done by operating the SpinCon II for a 4hr period
241 with a HEPA filter connected to the inlet which completely cleans the air entering the wet cyclone from
242 any bioparticles. All blanks were analyzed directly via FCM (Sect. 2.3) and EPM.

243 The volumetric flow rate within the SpinCon II was routinely calibrated by a VT100 Hotwire Thermo-
244 anemometer (Cole Palmer Inc.) using a 3-hole round duct transverse approach. A 1 ¼" OD tube with the
245 same diameter as the SpinCon II inlet was designed with 3 holes. Each hole was 60° apart from the other
246 and the holes were perpendicular to the axial air flow direction of the tube. (Supplementary Information,
247 Figure S1). Triplicates of flow rate measurements were taken in each hole at the center of the tube and
248 averaged to determine SpinCon II volumetric flow rate ($478.0 \pm 6.4 \text{ L min}^{-1}$).

249 **2.2 Flow Cytometry**

250 During this study, a BD Accuri C6 flow cytometer (BD Bioscience Inc.) was used for Flow Cytometry.
251 The instrument quantifies suspended cells in aqueous medium at three flow velocity modes (slow, medium
252 and fast flow at 14, 35 and 66 $\mu\text{L min}^{-1}$, respectively). It excites particles with a 488nm laser and possesses
253 four fluorescence detectors: FL1 (533±30nm), FL2 (585±40nm), FL3 (> 670nm) and FL4 (675±25nm),
254 which make it possible to analyze the fluorescence from multiple dyes concurrently. In this study, 2.5 μM
255 SYTO-13 nucleic acid probe was added to the fixed samples and incubated for 15min in the dark at room
256 temperature to stain biological particles. Additionally, 10 μL of 15 μm polystyrene bead suspension was
257 added to the 1mL total volume samples as an internal standard for PBAP concentration and size
258 quantification. The BD Accuri C6 was cleansed before each use with 0.2 μm filtered Milli-Q water in fast
259 mode for 10min; background particle counts were typically reduced to $1\mu\text{L}^{-1}$. At the beginning of every
260 experiment, a 1mL blank of the atmospheric sample without SYTO-13 and beads was analyzed, used in
261 quantification calculations (Sect. 3.1). Each sample was run in slow mode for 5min. After each sample, the
262 instrument was flushed with 0.2 μm filtered Milli-Q water in slow flow for 1 minute (important for robust
263 quantification of the typically low concentrations of the atmospheric samples). SYTO-13 fluorescence
264 intensity was quantified by the FL1-A detector and used in combination with other parameters (FSC-A &
265 SSC-A) to constrain the PBAP populations present. FSC-A measured forward ($0^\circ \pm 13^\circ$) scattering and is
266 used to characterize the size of particles; SSC-A measured the side ($90^\circ \pm 13^\circ$) scattering and is used to
267 characterize the internal complexity (non-sphericity/shape) of particles. A 80,000 unit intensity FSC-H

268 threshold (default FSC-H threshold value suggested by the manufacturer to minimize the effect of noise)
269 was set in the instrument during data acquisition to minimize the effects of noise on bioparticle counts. The
270 FSC-H channel (where H denotes height), measures single-particle forward scattering (FSC) intensity based
271 on the peak (maximum point) of the voltage pulse curve recorded when a single particle goes through the
272 interrogation point in the flow cytometer, whereas FSC-A, where A denotes area, measures single-particle
273 FSC intensity based on the area below the curve of the recorder pulse. When the 80,000 unit FSC-H
274 threshold is defined, only signals with an intensity greater than or equal to threshold value will be processed,
275 and this could affect the statistics and detection efficiency of the flow cytometer toward small particles (\leq
276 $1\mu\text{m}$). Experiments conducted with $1.0\mu\text{m}$ polystyrene beads suspension (Supplemental information;
277 Figure S16) have shown that $1.0\mu\text{m}$ beads have FSC-H intensities above the 80k threshold, no particle
278 losses is observed, and beads estimated concentration agree with the reported by the manufacturer ($\sim 6 \times$
279 10^7 mL^{-1} ; Life Technologies, Inc.) The FCM data from each sample was analyzed using the Flow Jo
280 software (<https://www.flowjo.com/solutions/flowjo>) to gate and quantify bioparticles population. The same
281 procedure was used to analyze the PBS, Milli-Q water and blanks.

282 **2.3 LIF detection of PBAP**

283 The WIBS-4A (referred to henceforth as “WIBS”) is a single biological particle real time sensor, which
284 measures particle light scattering and autofluorescence in an approximately $0.5 - 15\mu\text{m}$ particle range
285 (www.dropletmeasurement.com). Particles are initially sized using the 90-degree side-scattering signal
286 from a 635 nm continuous-wave diode laser. The scattering intensity is directly related to particle diameter
287 and was calibrated prior to deployment using polystyrene latex sphere calibration standards (PSL with 0.8,
288 0.9, 1.0, 1.3, 2.0, 3.0 μm diameter, Thermo Scientific Inc.). The WIBS optical size therefore refers to PSL
289 material with a real refractive index of 1.59. Healy et al. (2012) determined WIBS-4 counting efficiency by
290 aerosolizing standardized concentrations of PSL sphere of specific sizes (e.g. 0.3, 0.4, 0.56, 0.7, 0.9 and
291 $1.3\mu\text{m}$) and compared WIBS-4 total counts against PSL counts detected by the condensation particle
292 counter (CPC). Results show WIBS-4 possesses a 50% counting efficiency for $0.5\mu\text{m}$ particles and detects
293 100% of the PSL particles above $0.7\mu\text{m}$ when it is compared to the CPC counts. The 280nm and 370nm
294 pulsed Xenon flashtube UV lights in the WIBS cause the particles to autofluoresce (i.e., excite the
295 chromophores preexisting in the PBAP and do not rely on a fluorescent dye as done in FCM). Then,
296 fluorescent emissions are measured at three wavelength channels, which following the nomenclature of
297 Perring et al. (2015) are: (i) channel A (“FL1_280” in previous studies; Robinson et al., 2013), which refers
298 to the detected emission between 310-400nm after excitation at 280nm, (ii) channel B (“FL2_280” in
299 previous studies), which refers to the detected emission between 420-650nm after excitation at 280nm, and,
300 (iii) channel C (“FL2_370” in previous studies), which refers to the detected emission between 420-650nm
301 after excitation at 370nm. The resulting autofluorescence from 280nm excitation is affected by the presence

302 of tryptophan, tyrosine and phenylalanine amino acids in the PBAP (Pöhlker et al., 2012). Similarly, the
303 resulting autofluorescence from the 370nm excitation is influenced by the presence of riboflavin and co-
304 enzyme Nicotinamide Adenine Dinucleotide Phosphate (NAD(P)H) within the cells.

305 Biological and non-biological particles can be discriminated by using a fluorescent intensity threshold;
306 here the threshold is determined with the Gabey et al. (2010) method and with modifications by Perring et
307 al. (2015) as follows. Particles with fluorescence intensities below the fluorescence threshold in all channels
308 are categorized as non-fluorescent (NON-FBAP). Particles that fluoresce above the threshold in only one
309 channel are named with a single letter (e.g. A, B or C); particles that fluoresce in two channels are named
310 with the two channel letters (e.g. AB, AC or BC), while particles that fluoresce in all channels are
311 categorized as type ABC. Furthermore, the total FBAP concentration is defined as the sum of the
312 concentration in the seven FBAP categories defined above. This approach was applied by Hernandez et al.,
313 (2016) to pure culture PBAP (bacteria, fungal spores, pollen) to study their correspondence to FBAP types;
314 bacteria tend to be detected by type A, and fungal spores and pollen by type AB and ABC. However,
315 bioaerosol classification is instrument-specific and particle size dependent (Hernandez et al., 2016; Savage
316 et al., 2017). Multiple environments have been studied using the Perring et al. 2015 FBAP types, including
317 rural, urban and highly vegetated locations. In the Southeastern US, the total FBAP concentration range
318 from 2×10^4 to $8 \times 10^4 \text{ m}^{-3}$, constituting 3-24% of the total supermicron particle number between 1 and $10 \mu\text{m}$
319 diameter. In the highly vegetated Rocky Mountains, ABC type particles are enhanced during rainy days
320 (during or post-rain events) to ~ 65% of the total FBAP, owing to the release of wet-ejected fungal spores
321 following precipitation (Gosselin et al., 2016). On the contrary, in the highly populated city of Nanjing,
322 China all FBAP types, except type C, correlated with black carbon concentrations, suggesting a strong
323 interference by combustion sources (Yu et al., 2016). A detailed explanation of the above-mentioned studies
324 using Perring et al. 2015 approach is also included in the section SI.20 of the supplemental information.

325 **2.4 Location of sampling site and sampling frequency**

326 Bioaerosol sampling was conducted between April 7 and May 15, 2015 at the rooftop sampling
327 platform of the Ford Environmental Sciences and Technology (ES&T) building at the Georgia Institute of
328 Technology campus in Atlanta, GA. The site, which was located at the heart of a major urban environment,
329 is surrounded by dense forested areas in the southeastern USA: the Oconee National Forest (South East),
330 the Chattahoochee National Forest (North), and the Talladega National Forest (West). The WIBS was
331 operating continuously throughout the same period, sampling bioaerosol from a 15 ft. long and $\frac{1}{4}$ in. ID
332 conductive tubing inlet fixed 8 ft. above the sampling platform floor. The SpinCon II was placed in the
333 platform during sampling episodes with its inlet facing South. Three 4-hour samples per week were
334 collected with the Spincon II sampler over the 5-week period (4 h sampling between 10am and 5pm; Table

335 1). Meteorological data acquired from the same platform provided wind speed, wind direction, relative
336 humidity (RH), temperature, total hourly rain and UV radiation index with a 1min resolution.

337 **3. Data processing and Analysis**

338 **3.1 FCM data processing**

339 All blanks collected showed contamination levels that did not exceed 1% of the PBAP quantified in the
340 subsequent atmospheric samples. The 2-minute instrument blanks obtained after the CP and the HEPA filter
341 washes was $1.06 \times 10^3 \pm 7.37 \times 10^2 \text{ mL}^{-1}$ and $9.22 \times 10^2 \pm 1.24 \times 10^2 \text{ mL}^{-1}$, respectively, which are negligible
342 accumulations compared to the $2.55 \times 10^5 \pm 1.14 \times 10^5 \text{ mL}^{-1}$ average PBAP concentration quantified in the
343 atmospheric samples. The concentration of PBAP in the blanks was also confirmed with microscopy (not
344 shown). Based on this, we are confident that the CP protocol and procedure to replace the working fluids
345 ensured sterility of the biosampler before each sampling.

346 FCM analysis of the samples was carried out as follows. We obtain the fluorescence intensity (from
347 each of the 4 fluorescence detectors), forward scattering and side scattering intensity for all the particles
348 suspended in the samples. A gating procedure was used to determine the fluorescence levels associated
349 with detecting only particles containing SYTO-13 (hence, a PBAP) and background fluorescence from non-
350 stained particles. The procedure (Supplemental information, SI.2 and SI.3) consists of 3 steps: (a)
351 fluorescence threshold determination, (b) population gating, and, (c) biological/non-biological particle
352 discrimination in the population(s) within the threshold (e.g. LNA PBAP, Section 4.1). The fluorescence
353 threshold was determined using an atmospheric sample without SYTO-13 collected before each FCM
354 analysis, as a blank. Based on the fluorescence responses obtained, we determine the FL1-A fluorescence
355 intensity value for which 99.5% or 99.9% of the (unstained) particles of the blank autofluoresce below the
356 chosen value. This FL1-A intensity, called “fluorescence threshold”, was determined for each sample
357 (supplementary information, Figure S2a and S2b). The determination of the fluorescence threshold
358 involved selecting the most conservative value that maximizes inclusion of biological particles and
359 minimizes the inclusion of non-biological particles, including those that may be subject to background
360 fluorescence or unspecific binding of SYTO-13 (Diaz et al., 2010; Müller et al., 2010). We found out that
361 threshold values for the 99.9% approach were substantially higher than 99.5% approach in multiple
362 sampling events and comparable to the fluorescence intensities observed for stained pure cultures ($\sim 10^5$
363 units), which means that the 99.9% threshold values will miscount pure cultures as non-biological.
364 Consequently, we set the fluorescence threshold to the highest fluorescence intensity value observed by the
365 99.5% approach (41,839 units; supplementary information, Figure S2b), applied it to all collected samples;
366 henceforth named the 42k FL1-A threshold. The 42k threshold value aims to minimize any abiotic
367 interference as it maximizes biological particles quantification. A fixed value has been chosen and applied

368 to all samples given that having a different threshold value for each sampling event may result in
369 quantification biases as bioaerosols with strong autofluorescence (e.g. pollen, fungal spores) can increase
370 the threshold value and affect PBAP quantification in the population(s) within the threshold. The BD Accuri
371 C6 flow cytometer used for the analysis of the samples maintains constant pre-optimized photomultiplier
372 voltages and amplifier gain settings. As a result, the fluorescence intensity of particles is consistent from
373 day-to-day, and the fluorescence intensity of a specific biological particle population having the same
374 metabolic state and physiological characteristics must not show day-to-day variability
375 (www.bdbiosciences.com). Under the 42k threshold approach PBAP concentrations in the population(s)
376 within the threshold (e.g. LNA, Section 4.1) can be overestimated by up to a 0.5%. Furthermore, FCM
377 experiments conducted with unprocessed Arizona Test Dust (ATD) show that the FL1_A intensity
378 distribution of SYTO-13 stained ATD particles is very similar to unstained ATD particles, and 100% of the
379 SYTO-13 stained ATD particles stay below the 42k threshold (supplemental information, Figure S14a and
380 S14b), supporting the 42k threshold effectiveness to filter out abiotic particles.

381 Once the FL1-A threshold was determined, plots of FL1-A vs. SSC-A and FL1-A vs. FSC-A are used
382 to define clusters of bioparticles with fluorescence that exceed the FL1-A threshold and a characteristic
383 optical size (obtained from the FSC-A intensity) or particle shape/complexity (obtained from the SSC-A
384 intensity). FL1-A vs. SSC-A plots were used to define the populations of bioparticles for PBAP
385 quantification as clusters using SSC-A parameter were more defined and showed better spatial resolution
386 than using FSC-A parameter. The limits of each population were also determined with Flow Jo
387 (www.flowjo.com), using 2% contour plots (supplemental information; Figure S3) generated by equal
388 probability contouring (i.e., 50 contour levels so that the same number of cells fall between each pair of
389 contour lines). Populations above the FL1-A threshold value (41,839 FL1-A units) were considered
390 biological (Section 4.1; e.g. HNA); the particles in the population within the threshold value (Section 4.1;
391 e.g. LNA) having a FL1-A intensity greater than 41,839 units were counted as biological to determine the
392 PBAP counts in the population. The total PBAP counts were considered as all particles counts having FL1-
393 A fluorescence intensity above the determined threshold value minus the 15 μ m beads internal standard
394 having FL1-A fluorescence intensity above the determined threshold value. The 15 μ m beads of known
395 concentration and particle size allows for calibrating the optical size (supporting information, SI.7) of the
396 bioparticles, as well as their concentration and departure from sphericity. The 15 μ m beads population
397 showed fluorescence intensities comparable to the determined fluorescence threshold after been stained
398 with SYTO-13 as it is known that molecular stains can be adsorbed on the surface of polystyrene beads
399 (Eckenrode et al., 2005; Rödiger et al., 2011). The relatively high fluorescence intensity of the 15 μ m beads
400 show populations within the threshold value (e.g. LNA, Section 4.1) cannot be rule out as being affected

401 by unspecific staining of abiotic particles. However, populations above the threshold value (e.g. HNA,
402 Section 4.1) should not be affected by such abiotic interferences.

403 **3.2 WIBS data processing**

404 15-minute average total aerosol and FBAP size distributions were obtained from the WIBS. FBAP was
405 distinguished from the total aerosol using the Gabey et al. (2010) “trigger threshold” approach, which is
406 applied as follows. First, the average “electronic fluorescence noise” and its standard deviation is
407 determined for each channel (A, B, C) performing the Force Trigger (FT) calibration which consist to
408 operate the WIBS without flowing air through the system. The FT calibration, carried out every 24hr, is
409 critical for determining the lowest particle autofluorescence levels that robustly exceeds instrument
410 electronic noise. FT calibrations measured the particle-free air background autofluorescence in the three
411 WIBS channels (e.g. A, B, C), and measurements recorded the fluorescence intensity for 500 excitation
412 flash events (Ziemba et al., 2016; Tropak and Schnaiter, 2013; Gabey et al., 2010). The threshold for each
413 detector is then equal to the average fluorescence plus 2.5 times its standard deviation; particles with
414 fluorescence intensities above this threshold value are classified as FBAP. Then, Perring et al. (2015)
415 approach (Section 2.3) is applied to determine the combination of thresholds that provide the maximum
416 concentration of PBAP and minimal interference from abiotic particles, which still remains an area of active
417 research. It is important to note that the Gabey et al. (2010) threshold approach and the Perring et al. (2015)
418 FBAP types were applied to the WIBS-4A data and should not be directly compared to FBAP
419 quantifications performed by the WIBS-3 in previous studies, owing to the channel A and B overlap on the
420 latter. A detailed comparison between WIBS-3 and WIBS-4 models, as well as PBAP detection by both
421 models, is further discussed in the supplemental information (SI.20).

422 In this study, thresholds for each channel were determined daily, and the total particle concentration,
423 FBAP types (e.g. A, B, C, AB, BC, AC, ABC) concentrations and the total FBAP concentration (sum of
424 the seven FBAP types) were used. From the data, 4h-averaged size distributions (using 15-minute average
425 data) were generated for the total particles and all FBAP types in the 1-10 μ m range during the time SpinCon
426 II run. Subsequently, WIBS overall sampling efficiency (aspiration efficiency + transport efficiency) was
427 calculated using the Particle Losses Calculator (Von der Weiden et al., 2009) and applied to the 1-10 μ m
428 size distributions for the sampling characteristics in our setup (15ft. sampling line with ¼ in. ID and 2.3 L
429 min⁻¹ flow rate; Figure S4a). The sampling efficiency was calculated to be 67% for 5 μ m particles, with
430 larger losses as size increased to 10 μ m. (supplemental information, FigureS4b). FCM and WIBS total
431 particles and PBAP comparison was constrained to the 1 to 5 μ m range being the size overlap of both
432 techniques. Also, the fractional composition of FBAP (based on number concentrations) was calculated to
433 characterize its daily variability (Section 4.2), and compared against the daily variability of PBAP from the
434 FCM analysis (Section 4.4).

435 4. Results and Discussion

436 4.1 FCM biopopulation identification and quantification

437 When the FCM results are plotted in terms of FL1-A intensity versus SSC-A intensity, four populations
438 (Figure 2) emerge above the threshold gating process: low nucleic acid (LNA) particles, high nucleic acid
439 (HNA) particles, pollen and the 15 μ m internal standard beads. EPM and SEM pictures (Supplementary
440 Figures S5, S6, and S7) confirm the presence of these heterogeneous populations. Previously, LNA and
441 HNA populations were identified in FCM of aquatic samples with the use of the SYTO-13, SYBR green
442 and DAPI nucleic acid stains (Wang et al., 2010; Bouvier et al., 2007; Lebaron et al., 2001); corresponding
443 populations in atmospheric PBAP have not been identified before. Below we focus on each population to
444 further understand the identified populations of biological particles.

445 The HNA size distributions are dominated by 3-5 μ m particles (mean diameter: $4.15 \pm 0.06 \mu$ m;
446 Supplemental Information, Figure S10) and the total concentration moderately correlated with RH. HNA
447 were virtually non-existent during several extended dry periods (days with average RH < 70% during
448 sampling, e.g. 4/9, 4/22 and 5/15) and well defined during periods of high humidity, especially after rain
449 events (days with average RH > 70% and T > 18 °C during sampling episode; e.g. 4/7, 4/14, 4/15). Both of
450 these characteristics suggest that HNA particles correspond to wet-ejected fungal spores (e.g., from the
451 Ascospores and Basidiospores genus; Oliveira et al., 2009; Li and Kendrick, 1995). The LNA size
452 distributions are dominated by 2-4 μ m particles (mean diameter: $2.99 \pm 0.06\mu$ m; Supplemental Information,
453 Table S1) and dominated Atlanta PBAP composition during dry days. Many individual bacteria are likely
454 in around 1 μ m, but the observed LNA particles are within the median aerodynamic diameter of culturable
455 bacteria (~ 4 μ m) in continental sites (Despres et al., 2012). Bacteria in the atmosphere can be co-emitted
456 together with larger particles (e.g. soil, plant fragments) and occasionally they are observed as clumps of
457 bacteria cells (Burrows et al., 2009). In addition, several bacterial species observed in the atmosphere
458 (Delort and Amato, 2018; Monier and Lindow, 2003; Baillie and Read, 2001) are within this sizes range
459 (e.g., *Sphingomonas spp.*: 1.0 - 2.7 μ m; *Methylobacterium spp.*: 1- 8 μ m, *Pseudomonas syringae*: ~2.5 μ m,
460 and *Bacillus anthracis*: 3-10 μ m), supporting LNA population may represent single or agglomerated
461 bacterial cells. However, it is clear that heterogeneous populations will probably contain multiple types of
462 microorganisms and that may be the case in the LNA population. The LNA population also shows SYTO-
463 13 fluorescence intensities that are about one order of magnitude lower than the HNA population.

464 It is known that pollen may burst into tiny fragments when is suspended in water (e.g., Augustin et al.,
465 2012; Taylor et al., 2007), potentially increasing the concentration of LNA particles and biasing
466 concentrations. Although 0.2 μ m – 5 μ m pollen fragments can be generated upon rupture, pollen (e.g. Birch,
467 Ryegrass, Oak, Olive) mainly breaks apart into submicron fragments by hydrolysis and favors

468 fragmentation into small submicron ($<1\mu\text{m}$) particles (Taylor et al., 2007; Bacsi et al., 2006; Grote et al.,
469 2003), not considered in our FCM analysis. An additional factor to consider in pollen fragmentation is the
470 number of fragments generated per pollen grain. FCM applied to ragweed pollen suggests a 1:2 pollen-to-
471 pollen fragments concentration ratio (Supplementary information, Table S2). Also, calculations based upon
472 FCM-derived ragweed pollen and pollen fragments concentrations during this study (considering the total
473 pollen mass added to the sample, $15\mu\text{m}$ mean diameter previously determined by Lin et al. (2013) and unit
474 density) suggest approximately 67% of the ragweed pollen grains were intact after hydration and that each
475 fragmented grain generates ~ 5 pollen fragments; in agreement with Bacsi et al. (2006), 35% of ragweed
476 pollen fragments upon hydration. Overall, ragweed pollen results suggest FCM experiments do not have a
477 considerable impact in pollen fragmentation and that pollen fragmentation will have a negligible effect on
478 LNA concentrations. Ragweed pollen is one of the most abundant wind-driven pollen species in the United
479 States and its emission peaks during fall, but can be also present during late spring and summer. It is
480 representative of the pollen species we see in the Atlanta area (Darrow et al., 2012) and results suggest
481 pollen fragmentation would not generate a substantial amount of fragments. The low collection efficiency
482 of SpinCon toward large particles ($<14\%$ for diameters above $5\mu\text{m}$) and that pollen concentrations in our
483 samples are generally two orders of magnitude lower than LNA concentrations (Figure S22; supplemental
484 information) suggest a negligible effect of pollen fragments in LNA biological particle quantification.
485 Pollen concentrations are 100-1000 times lower than bacteria concentrations in the atmosphere (Hoose et
486 al., 2010). At least 100 supermicron ($>1\mu\text{m}$) pollen fragments will have to be released per pollen grain to
487 considerably influence the LNA population, which has not been observed. Also, EPM results showed intact
488 pollen and limited amounts of small debris among the particles identified in the atmospheric samples
489 collected for this study. Particles with fluorescence intensities above the FL1-A threshold value in the LNA
490 population were counted as biological, giving us the PBAP counts within the LNA population and will be
491 referred henceforth as the “LNA-AT” population (Figure 2), where “AT” refers to above threshold.

492 A population of strongly fluorescing and very large particles ($10\text{-}20\mu\text{m}$, avg. average geometric mean
493 diameter $12.3 \pm 1.7\mu\text{m}$) was identified (Figure 2). This population also strongly autofluoresces in the FCM
494 when SYTO-13 was not added to the sample (SI.7, Figure S11). All together this indicates a population of
495 pollen particles, as they are known to contain cell wall compounds (i.e., phenolic compounds, carotenoid
496 pigments, Phenylcoumarin) that fluoresce more strongly than the proteins and cytosolic compounds
497 responsible for bacteria/fungi autofluorescence (Pöhlker et al., 2012; Hill et al., 2009; Pöhlker et al., 2013).
498 The pollen population was not well-defined during all sampling events; whenever present, pollen was
499 characterized by concentrations ($\sim 10^2 \text{m}^{-3}$) consistent with reported values (Despres et al., 2012), which are
500 also much lower than LNA-AT and HNA concentrations. As a result, pollen population was systematically
501 gated using a perfect square between 10^6 and 10^8 intensity units in the FL1-A vs. SSC-A plot for each

502 atmospheric sample. LNA-AT, HNA and pollen counts, acquired by the 42k threshold approach were used
503 to calculate liquid-based (mL^{-1} of sample solution) and air-based (m^{-3} of air) concentrations for each
504 bioaerosol population as detailed in the Supplemental Information. The total PBAP concentration on each
505 sample consisted of all non-bead particles above the 42k fluorescence threshold given that a non-negligible
506 biological particle concentration was not constrained in the gated populations. Even though the 2% contour
507 plots effectively allowed population gating, $16.5 \pm 7.3\%$ of the total PBAP are not attributed the identified
508 populations. The biological particles not constrained by FlowJo 2% gating, henceforth named as the
509 “unclassified” bioparticles, showed the highest concentrations when both HNA and LNA populations are
510 densely populated (4/16, 4/28 and 5/14; Figure 5). The lowest concentrations were observed when just the
511 LNA population is identified (4/9, 4/22, 5/15; Figure 5) and when the LNA and HNA populations are
512 identified after the rain event on 4/14. The observed behavior shows that the unclassified bioparticle
513 concentrations is linked to the heterogeneity of the biological populations and the concentration of the gated
514 populations (e.g. HNA, LNA and Pollen). The “unclassified” bioparticles concentration ranges from $8.1 \times$
515 10^2 m^{-3} to $1.3 \times 10^4 \text{ m}^{-3}$ (avg. $4.2 \times 10^3 \pm 3.3 \times 10^3$) and they are not constrained to a specific size range.
516 Most of the unclassified bioparticles are far from the centroids of the gated populations. They can indeed
517 be formed by fragmentation or accretion, or also be related to plant debris (i.e., irregular bioparticles) that
518 are characterized by a very broad size, internal complexity and nucleic acid content distributions. In
519 addition, we must note that additional concentration corrections are required owing to the sampling
520 efficiency of the SpinCon II, but will be considered in sections 4.3 and 4.4.

521

522 Before SpinCon II sampling efficiency corrections are applied, FCM total particle concentrations range
523 from $2.6 \times 10^4 \text{ m}^{-3}$ to $2.9 \times 10^5 \text{ m}^{-3}$, with increasing concentrations toward the end of the sampling period.
524 In addition, total PBAP concentration averaged $2.4 \times 10^4 \pm 1.1 \times 10^4 \text{ m}^{-3}$ (coefficient of variation, CV, 13%;
525 defined as the standard deviation over a triplicate FCM measurements over the average concentration).
526 LNA-AT ranged between 6.8×10^2 and $2.9 \times 10^4 \text{ m}^{-3}$ (average: $1.1 \times 10^4 \text{ m}^{-3}$; CV: 20%), HNA (fungal spores)
527 between 4.7×10^3 and $1.9 \times 10^4 \text{ m}^{-3}$ (average: $1.1 \times 10^4 \text{ m}^{-3}$; CV: 15%) when above the detection limit ($n=12$),
528 and pollen from 1.3×10^2 to $1.2 \times 10^3 \text{ m}^{-3}$ (average: $3.6 \times 10^2 \text{ m}^{-3}$; CV: 21%). These concentration levels are
529 consistent with microscopy-based studies in urban environments for bacteria (e.g., $1.7 \times 10^4 \pm 1.3 \times 10^4 \text{ m}^{-3}$
530 in springtime Birmingham, UK; (Harrison et al., 2005); fungal spores ($1.8 \times 10^4 \pm 1.1 \times 10^4 \text{ m}^{-3}$ in Vienna,
531 Austria between April-June; Bauer et al., 2008); and pollen (between $5.69 \times 10^2 \text{ m}^{-3}$ to $6.144 \times 10^3 \text{ m}^{-3}$ in
532 Medellin, Colombia; Guarín et al., 2015). Also, additional experiments performed in September 2015,
533 described in Figure S7 of the supplemental information (supplemental information, SI.6), showed that EPM
534 and FCM-based quantifications agree within an order of magnitude. This is consistent with Lange et al.

535 (1997), whom also found that FCM gives higher quantifications than EPM microscopy when studying *P.*
536 *aeruginosa* pure cultures and airborne bacteria collected from a swine confinement building in Iowa, USA.

537 To better understand SYTO-13 fluorescence intensity differences between the identified (e.g. LNA-
538 AT, HNA and pollen) populations in the atmospheric samples and their metabolic/stress state, FCM
539 experiments were conducted with air-isolated bacteria (F8 strain; De Leon Rodriguez, 2015), ragweed
540 pollen and yeast (*S. cerevisiae*; Y55 strain) mixtures to compare the SYTO-13 fluorescence intensity and
541 the scattering properties of the pure cultures to those seen in the atmospheric samples. Pure cultures and
542 atmospheric samples are summarized in Tables S3, S4 (supplementary information; FCM pure culture
543 experiments) respectively. The LNA-AT population showed SYTO-13 fluorescence intensity up two orders
544 of magnitude lower than F8 bacteria. HNA (fungal spores) population showed an order of magnitude lower
545 SYTO-13 fluorescence intensity than Y55 HNA yeast, and, within the same magnitude for the LNA Y55
546 yeast. The HNA and LNA yeast populations in the pure culture experiments (Figure S13a) have one order
547 of magnitude difference in FL1-A fluorescence intensity and may represent yeast populations with different
548 metabolic states. Atmospheric and ragweed pollen populations had similar SYTO-13 fluorescence
549 intensities and Figure S13c shows pollen fluorescence intensity may go up to 10^8 . The lower SYTO-13
550 fluorescence intensity of the atmospheric populations may be related to genetic material degradation from
551 exposure to atmospheric stressors; depending on the physiological characteristics of each population (Zhen
552 et al., 2013; Amato et al., 2015). Our results also agree with Guindulian et al. (1997), showing that *E.coli*
553 overnight cultures have higher SYTO-13 fluorescence intensity than starved *E.coli* population. Overall,
554 FCM pure culture results suggest microbes starve in the atmosphere, leading to a possible reduction or
555 leakage of the amount genetic material enclosed within each cell. Sampling can also stress cells, even
556 disrupt the wall/membrane of the cell and lead to genetic material leakage (Zhen et al., 2013).

557 Pollen, HNA and LNA-AT atmospheric populations showed different SYTO-13 fluorescence
558 intensities. Pollen showed the highest fluorescence intensity, followed by the HNA and LNA-AT (fraction
559 of LNA above threshold; Figure 2) populations, respectively (Figure 2; Table S4). Guindulian et al. (1997)
560 FCM results with starved bacterioplankton from seawater samples treated with DNase/RNase showed
561 SYTO-13 fluorescence intensity can be related to the DNA content of starved bacterioplankton due to the
562 low amount of RNA enclosed in starved cells. Taking in consideration our results and previous studies, we
563 can suggest that Pollen, LNA-AT and HNA populations in the atmospheric samples are differentiated by their
564 DNA content, which can in part explain SYTO-13 fluorescence intensity difference between them. We also
565 acknowledge DNA sequestration by bacteria, fungal spores and pollen may differ and their cell membrane
566 characteristics will ultimately determine how much stress the cells will sustain before they completely
567 rupture. SYTO-13 is a highly permeable stain and effectively detects nucleic acids (DNA and RNA) of

568 bacteria endospores and vegetative cells (Comas Riu et al.,2002). Fungal spores have also been effectively
569 stained by DNA/RNA probes (Bochdansky et al., 2017; Chen and Li et al., 2005), but some fungal spores
570 might not be equally stained due to their harder cell wall, and chromatin-binding of DNA (Standaert-Vitse
571 et al., 2015). Future work is needs to further study this.

572

573 **4.2 WIBS total concentration and FBAP daily variability**

574 WIBS-4A collected data continuously throughout the period; for comparison against the SpinCon
575 II 4h liquid batch samples, WIBS data was averaged to the SpinCon II sampling times (Table 1). WIBS
576 total particle concentration (1-5 μ m diameter) ranged from 2.0×10^5 to 1.0×10^6 m^{-3} in agreement with
577 observed particle concentrations in previously studied urban environments during Spring/Summer months
578 like Helsinki, Finland (UV-APS avg. 1.6×10^5 m^{-3} ; Saari et al., 2014) and Karlsruhe, Germany (WIBS-4
579 avg. 6.9×10^5 m^{-3} ; Tropak and Schnaiter et al., 2013). 4h average total particles concentrations in Figure 3a
580 show particle concentrations declined during rain episodes (during or post-rain: e.g. 4/15, 4/16, 4/28, 4/29,
581 4/30) as wet removal of PBAP is most efficient. However, during dry (no rain) episodes total particle
582 concentrations built up in the atmosphere. To better understand the day-to-day variability of different FBAP
583 types, the seven Perring et al. (2015) FBAP categories (e.g. Type A, B, C, AB, AC, BC and ABC) were
584 studied plus the NON-FBAP type constituting particles that do not fluoresce in any channel (e.g. channel
585 A, B, C). NON-FBAP concentrations are one order of magnitude higher than FBAP concentrations, and
586 NON-FBAP, hence traced WIBS total particles throughout all sampling events (Figure 3a). Total FBAP
587 concentrations also show similar behavior to the total particle concentration (Figure 3a) and it suggests non-
588 biological particles can be biasing the total FBAP concentration. The variability of the total FBAP
589 concentration is mainly linked to type A and type B concentrations as overall they constitute the two largest
590 fractions to the total FBAP concentration (Figure 3b), and both FBAP types have previously misidentified
591 non-biological particles as FBAP (Tropak and Schnaiter et al., 2013; Yu et al., 2016). As a result, our study
592 considers the total FBAP concentration as the upper limit, and ABC type concentration as the lower limit
593 of FBAP concentration in Metro, Atlanta. Type B dominates the FBAP fractional composition (Figure 3b),
594 which has been linked to possible non-biological interferences from black carbon (Yu et al., 2016) and
595 polycyclic aromatic hydrocarbons (PAHs) emitted from combustion sources. Total FBAP fraction ranges
596 from 16% and 43%, and ABC fraction ranges from 1.3% and 9.2% of the total particles in the 1 to 5 μ m
597 size range. ABC type fractions and ABC type concentrations are within the values observed by Tropak and
598 Schnaiter (2013) using WIBS-4 in Karlsruhe, Germany; averaging 2.9×10^4 m^{-3} (when considering the sum
599 of AC and ABC types) and constituting 7% of total coarse mode particles (0.8 μ m-16 μ m).

600 ABC type concentrations show an interesting variability throughout the 15 sampling events, as
601 ABC reaches its maximum concentration on 4/14, on a warm and humid day after a rain event, concurrently
602 when the FCM HNA population also reaches its highest concentration – strongly suggesting ABC particles
603 are fungal spores. (Figure 3a, Table 1). Recently, Gosselin et al. (2016) used WIBS-3 in the Rocky
604 Mountains, Colorado showing ABC type fractional composition enhances after rain events to dominate the
605 total FBAP composition and the enhancement is correlated to mannitol and arabitol concentrations (fungal
606 spore tracers), which have been previously linked to Ascomycota and Basidiomycota spores emitted by the
607 wet-ejection mechanism (Elbert et al., 2007). In addition, ABC type constitute a considerable fraction
608 (~20%) of total FBAP during dry days in the Rocky Mountains possible because such highly vegetative
609 environments maintain a high background of fungal spores (Huffman et al., 2013). However, urban
610 environments like Metro Atlanta are not necessary dominated by fungal spores and its FBAP composition
611 will be affected by the biological sources close to city (e.g. forests), local emissions and meteorology. The
612 overall FBAP composition in metro Atlanta (Figure 3b) is dominated by type B (avg. fraction: $33 \pm 9\%$),
613 type A (avg. fraction: $22 \pm 5\%$) and type AB (avg. fraction: $22 \pm 5\%$) particles. Type ABC constitute $12 \pm$
614 6% of the total FBAP and it reaches 30% on 4/14, comparable to values observed by Gosselin et al., 2016
615 in the Rocky Mountains. The dominance of type B particles has been observed in the polluted atmosphere
616 of Nanjing, China using WIBS-4A were type B constituted ~ 45% of the total PBAP and type B ($\sim 2 \times 10^6$
617 m^{-3}) concentrations were up to two orders of magnitude higher than type A concentrations ($\sim 5 \times 10^4$ m^{-3})
618 suggesting a high likelihood of interference from abiotic particle sources. However, Metro-Atlanta shows
619 much lower total particle concentrations than Nanjing, China ($\sim 10^7$ m^{-3}) and type A and type B
620 concentrations are within the same order of magnitude. Furthermore, Perring et al. (2015) have shown type
621 B particles constitute a considerable fraction of the total supermicron particles across the United States,
622 being ~15% and ~25% over (altitude >100m) the Southeastern US and Southwestern US, respectively.
623 Total particle and NON-FBAP size distributions in Figure 3c peaked at $\sim 1\mu\text{m}$. Similarly, types A, B, AB
624 size distributions (Figure 3d) peaked close to $1\mu\text{m}$ showing that interferences by non-biological particles
625 cannot be rule out. However, ABC type size distribution (red line, Figure 3d) is dominated by $3\text{-}5\mu\text{m}$
626 particles and ABC type particles may have come from a different source to other FBAP types as they get
627 enhanced after rain events (e.g. 4/14; Table 1). Yu et al. (2016) also observed $4\text{-}6\mu\text{m}$ ABC type particles
628 in the highly polluted Nanjing, China, but ABC type bimodal size distributions showed a peak between 1-
629 $2\mu\text{m}$ and a second peak between $4\text{-}6\mu\text{m}$. In addition, ABC type number fractions in Nanjing, China
630 correlated to black carbon mass fractions suggesting a considerable influence by combustion related
631 particles and no rain events occurred during the sampling period. The difference between Metro Atlanta
632 and Nanjing, China ABC type size distributions suggest ABC type is not influenced by combustion related
633 particles in Metro Atlanta. Overall, results show FBAP concentration ($1\text{-}5\mu\text{m}$) ranges from 10^4 - 10^5 m^{-3} in

634 metro Atlanta and wet-ejected fungal spores concentration, detected by ABC type, can constitute up to 30%
635 of the FBAP (1-5 μm) after rain events.

636 **4.3 Correlation of HNA population with ABC type**

637 A quantitative comparison between WIBS-4A total particle and FCM total particle concentrations
638 was subsequently performed and we focused the analysis to the 1 to 5 μm size range as SpinCon sampling
639 efficiency is reduced significantly above 5 μm ($\leq 14\%$; Kesavan et al., 2015). WIBS-4A and FCM total
640 particle concentrations differed by about one order of magnitude (for optical diameter, d_o , greater than
641 1.5 μm) and particle concentration difference increased for particles with $d_o < 1.5 \mu\text{m}$ as shown in the size
642 distribution (geometrically averaged across the 15 SpinCon II sampling events) in Figure 4a. The largest
643 difference between WIBS-4A and uncorrected FCM size distributions seems to be related to SpinCon II
644 having a cutoff size close to 1 μm , reducing significantly its sampling efficiency. Even with the observed
645 difference in the magnitude of the concentrations between the two techniques, ABC type and HNA
646 concentrations traced throughout all the sampling events and are moderately correlated ($R^2 = 0.40$, P-value
647 = 0.016; Figure 4b) and showed similar size distributions in the 1 to 5 μm range as shown in Figure S12a.
648 HNA and ABC type were both dominated by 3-5 μm particles and it seems both are detecting the same
649 type of biological particles. In addition, AB type showed a weak correlation with HNA concentrations (R^2
650 = 0.17), but their size distributions differed as type AB peaks close to $\sim 1\mu\text{m}$ (Figure 3d). ABC is the only
651 FBAP type showing a considerable correlation to the HNA population, and LNA-AT population is not
652 correlated with any FBAP type. Overall, ABC type and HNA correlation is an important step forward to
653 better understand the effectiveness of WIBS-4A FBAP categories to provide speciated PBAP
654 concentrations in urban areas. ABC type particles have shown substantial concentrations (10^4 - 10^5 m^{-3} ;
655 Perring et al., 2015; Ziemba et al., 2016) across the US. The highest ABC fraction of the total FBAP was
656 observed in Panhandle, Florida during an airborne study among multiple environments studied using
657 WIBS-4A to sample from the California coast to central Florida, suggesting ABC type particles are
658 ubiquitous in the US (Perring et al., 2015). Previous studies (Healy et al., 2014, Huffman et al., 2013) have
659 shown correlations between LIF technology (e.g. WIBS-4 and UV-APS) fluorescence channels and fungal
660 spores number concentrations, especially during fungal spores invigoration after rain events. Healy et al.
661 (2014) used WIBS-4 in Killarney National Park, Ireland (e.g. high vegetative rural area) finding correlations
662 between channel B (FL2; $R^2 = 0.29$) and channel C (FL3; $R^2 = 0.38$) concentrations and fungal spores
663 concentrations (collected by Sporewatch impactor and quantified by microscopy). However, now for the
664 first time FCM HNA population have shown a correlation with WIBS-4A ABC type and suggests ABC
665 type category detects wet actively ejected fungal spores in Metro Atlanta (e.g. urban area). In addition,
666 recent WIBS-4A experiments using pure cultures have shown ABC type detects well several fungal spores

667 (e.g. *Aspergillus Versicolor* & *Botrytis spp.*) and small pollen grains, but detection may vary across
668 instruments (Hernandez et al., 2016).

669 FCM concentrations were corrected based on correction factors (CF) calculated upon the
670 comparison of ABC and HNA size distributions (1 to 5 μ m) for each sampling event given (1) ABC type
671 and HNA population similar size distributions and number concentrations (1 to 5 μ m) correlation, and, (2)
672 WIBS-4A provides us representative concentrations of airborne particle concentrations in Metro Atlanta
673 after sampling losses being corrected (Section 3.2). Concentration correction factors were determined for
674 each sampling episode by taking the quotient of ABC type to HNA concentrations over the 1-5 μ m size
675 range. The resulting size-dependent correction factor (Figure S12b) was then applied to the FCM size
676 distributions, giving the “corrected FCM” bioaerosol data (between 1 and 5 μ m). Figure 4a shows that the
677 corrected FCM total particle average size distribution traces WIBS-4A size distribution, allowing us to
678 correct for SpinCon II low collection efficiency and to better constrain the magnitude of FCM
679 concentrations. Our approach to calculate the estimated collection efficiency (ECE) considers all the
680 processes that affect the concentration of PBAP, from collection to final quantification in the FCM. Figure
681 S12b compares Kesavan et al. (2015) collection efficiencies determined for SpinCon I and the estimated
682 collection efficiency calculated upon the CF calculation ($ECE = 1/CF$) and shows the ECE of the SpinCon
683 II is lower than Kesavan et al. (2015) below 3 μ m and performs better for particles above 3 μ m, but above
684 3 μ m Kesavan et al (2015) collection efficiency is within the uncertainty of our calculations. Our lower ECE
685 values (Figure S12b) for particles below 3 μ m can be related to SpinCon sampling time as Kesavan et al.
686 (2015) experiment were conducted in a short period of time (e.g. 10-15 min) and ours took place for 4 h
687 The main mechanisms leading to below 3 μ m particle losses could be their re-aerosolization over time being
688 lost through the blower exhaust of the SpinCon II (Figure 1). Also, coagulation of small particles over time
689 can not be rule out, but future work is needed to study it.

690

691 **4.4 PBAP populations after collection/detection corrections**

692 After correction through the application of the ABC correction factors, FCM total particle
693 concentrations (1 to 5 μ m avg.: $5.5 \times 10^5 \pm 5.1 \times 10^5 \text{ m}^{-3}$; Figure 5a) are within the same order of magnitude
694 as WIBS-4A concentrations (1 to 5 μ m avg.: $5.4 \times 10^5 \pm 2.9 \times 10^5 \text{ m}^{-3}$; Figure 3a), and continue to exhibit
695 substantial variability. The HNA (e.g. fungal spores) population showed a substantial invigoration during
696 three sampling events (4/7, 4/14, 4/15; Figure 5a and 5b). To better understand the role of meteorology on
697 PBAP composition, the PBAP samples were classified into four regimes based on the average diurnal
698 relative humidity and ambient temperature, with $T = 18 \text{ }^\circ\text{C}$ (65 $^\circ\text{F}$) to differentiate between warm and cold
699 days, and, $RH = 70\%$ to differentiate between humid and dry days. The temperature and RH threshold

700 values were chosen based on the observations and understanding that a combination of temperature and RH
701 within these threshold values can significantly impact bioaerosol composition. For instance, humid and
702 warm conditions may lead to the invigoration of fungal spores by wet ejection from plants (Ingold, 1971),
703 on contrary, PBAP will get stressed when exposed to warm and dry conditions. The sampling times, RH,
704 ambient temperature and meteorological categories of each SpinCon II sample is presented in Table 1.

705 Humid and warm days (4/7, 4/14 and 4/15; light green shaded areas in Figure 5a) were characterized
706 by well-defined HNA and LNA-AT populations. These sampling episodes had the highest average HNA
707 (fungal spore) concentration ($4.0 \times 10^4 \pm 1.3 \times 10^4 \text{ m}^{-3}$) among the four meteorological regimes and during
708 these sampling events HNA constituted $\geq 77\%$ of the total PBAP. Among the humid and warm days (Figure
709 5a and 5b), average LNA-AT, HNA and “unclassified” bioaerosol compositions were 6.1%, 84.0% and
710 9.9%, respectively of the total PBAP number. Also, the humid and warm days occurred after rain events,
711 which can be linked directly to the strong fungal spore invigoration (Huffman et al., 2013). Before sampling,
712 early morning precipitation occurred during 4/14 and 4/15, as well as during the night of 4/6. Precipitation
713 did not occur during sampling in any of the humid and warm days. The FCM results (Figure S15a-c) that
714 display the PBAP population between 4/7 and 4/9 show a disappearance of the (HNA) fungal spore
715 population during the transition from a “humid and warm” day (4/7) to a “dry and warm” day (4/9). Figure
716 5b shows how the HNA contribution to the total PBAP goes down on 4/8 when RH decreases and is
717 undetected on 4/9. Furthermore, Figure 6a-c shows FL1 vs. SSC-A plots for 4/14 to 4/16 consecutive
718 sampling periods, where a marked increase in the LNA-AT concentration from 4/15 to 4/16 goes together
719 with a striking decrease in the HNA concentration. HNA fraction went down from 92.0% to 34.1% of the
720 total PBAP and LNA-AT concentration went up from $3.8 \times 10^3 \text{ m}^{-3}$ to $2.9 \times 10^4 \text{ m}^{-3}$. Humid and Warm days
721 had the lowest averaged PBAP concentration ($4.6 \times 10^4 \pm 9.8 \times 10^3 \text{ m}^{-3}$ in the 1 to $5\mu\text{m}$ range) among the
722 four meteorological regimes, a possible effect of the bioaerosols being lost by wet scavenging, resulting in
723 the enhancement of fungal spore contribution to the total PBAP number concentrations. The unclassified
724 biological particles concentration also showed its lowest contribution ($2.9 \times 10^3 \text{ m}^{-3}$; 9.9%) to the total
725 PBAP number concentration during these events, when the HNA and LNA populations are best identified
726 by the 2% contour plots.

727 Cold and humid days (4/16 and 4/29; light yellow shaded areas in Figure 5a) also showed well-defined
728 HNA population, and HNA contributed on average to $29.5 \pm 6.5\%$ of the total PBAP concentration (1 to
729 $5\mu\text{m}$). On 4/16 drizzling took place by the end of the sampling period, but no accumulated rainfall was
730 measured by the meteorological station. However, on 4/29, accumulated rainfall averaged 0.04in. from
731 11:55 AM to 2:20 PM (Figure S21). The similar HNA concentration between “Humid and Warm” and
732 “Humid and Cold” days seen in Figure 5a and the lower contribution of HNA to the total PBAP during the

733 “Humid and Cold” days may be linked to previously suggested bacteria emissions by droplet soil impaction
734 during rain events (Joung et al., 2017). Bacteria emission by soil impaction can increases airborne LNA-
735 AT concentration and HNA (fungal spores) will have a lower contribution to the total PBAP even when the
736 fungal spore concentration is high during rain events. Both cold and humid days showed a considerable
737 difference in LNA-AT contributions to the total PBAP concentration. On 4/16 and 4/29 LNA-AT
738 constituted 45.2% and 65.3% of the total PBAP concentration, respectively (Figure 5b). The difference in
739 the LNA-AT contribution to the total PBAP can be linked to the intensity of precipitation, as it shapes the
740 composition (e.g. size and types) of microbes suspended in the atmosphere during the different stages of a
741 rainfall (e.g. before, on set, during and after a rainfall; Yue et al., 2016).

742 Six of the fifteen sampling days were classified as warm and dry (4/8, 4/9, 4/22, 5/13, 5/14, 5/15; light
743 orange shaded areas in Figure 5a) and it did not rain before or during any of these days (Table 1). During
744 warm and dry days, HNA had the lowest averaged concentration ($8.7 \times 10^3 \pm 1.2 \times 10^4 \text{ m}^{-3}$) among the four
745 meteorological categories. In addition, during three dry and warm days (4/9, 4/22 and 5/15) the HNA
746 population was undetected. This behavior can be related to the fact that high RH drives fungal spore
747 emissions by wet ejection, but soil wetness could also affect emissions because the HNA population was
748 detected in other warm and dry days with comparable RH (Huffman et al., 2013; Gosselin et al., 2016). The
749 air mass trajectories reaching Atlanta during each sampling event could also affect the biological particles
750 composition. For example, on 4/22, when the HNA was undetected, the 500m and 100m 72 h backward air
751 mass trajectories reaching Atlanta came from the NW (US/Canada border) at high altitudes and do not
752 spend more than 24h near surface. This air mass could affect bioaerosol composition with minimal
753 influence from local bioaerosol emissions. However, the enhancement or the depletion of the HNA
754 population have not been linked to specific air masses trajectories. Besides meteorology, two main
755 hypotheses could explain the observed behavior in the HNA population, previously stated by Bouvier et
756 al., 2007 to understand HNA and LNA populations in aquatic environments, but also applicable to airborne
757 microorganisms. First, microbes might begin in the HNA population upon aerosolization and then move to
758 the LNA upon death or inactivity. Second, the HNA and LNA populations may contain completely different
759 microbial taxa and have different organisms in each population. If the first hypothesis occurs, we expect to
760 see a covariance of the HNA and LNA FCM parameters (e.g. FSC-A, SSC-A and FL1-A intensities), and
761 observe a gradual decrease in the FL1-A intensity of the HNA population to the FL1-A values observed by
762 particles in the LNA population, which is not seen. Although our results suggest the HNA and LNA are
763 two distinctive populations, further studies will have to take place to sort and directly study the DNA
764 sequences of each population in order to prove the second hypothesis. HNA population behavior may also
765 consist of a combination of both hypotheses. Overall, warm and dry days prevail during springtime in

766 Atlanta and LNA-AT contribution (avg.: $3.4 \times 10^4 \pm 2.5 \times 10^4 \text{ m}^{-3}$) may represent the bioaerosol background
767 of Atlanta.

768 Four of the fifteen sampling days (4/21, 4/23, 4/28 and 4/30; light blue shaded areas in Figure 5a) were
769 characterized by cold and dry conditions (Table 1). PBAP were dominated by LNA-AT during these events,
770 as can see in Figure 7a-c, where LNA population are the dominant contributors to PBAP number. HNA
771 population was diminished in Figure 7a (4/21) & Figure 7c (4/23) during cold and dry days and disappeared
772 in Figure 7b during a warm and dry day. Overall, HNA was detected during cold and dry days, but showed
773 lower contributions to the total PBAP number concentration than humid days. Among cold and dry days,
774 the PBAP population (1 to 5 μm) was composed on average of $72.6 \pm 10.1\%$ LNA-AT and $16.5 \pm 8.2\%$
775 HNA. Cold and dry days had on average the highest LNA-AT ($5.3 \times 10^4 \pm 1.8 \times 10^4 \text{ m}^{-3}$) and total PBAP
776 ($7.3 \times 10^4 \pm 2.0 \times 10^4 \text{ m}^{-3}$) number concentrations (1 to 5 μm) among the four meteorological categories,
777 reaching the PBAP maximum concentration on 4/23 (Figure 5a).

778

779 **4.5 PBAP day-to-day variability in Metro Atlanta: FCM vs. WIBS**

780 Although WIBS and FCM possess different methodologies, they show similar trends providing a
781 good understanding of the daily variability of PBAP in Metro Atlanta. FCM PBAP fraction (1 to 5 μm)
782 ranges from 3.8% to 69.2% of the total particles and the highest PBAP fraction (69.2%) and HNA
783 concentration is observed on 4/14 ($5.25 \times 10^4 \pm 5.89 \times 10^3 \text{ m}^{-3}$). The total FBAP fraction (1 to 5 μm) ranges
784 from 16% to 43%, but it reaches its maximum on 4/15. However, ABC fraction of the total WIBS particle
785 concentration ranges from 1.3% to 9.2% and it reaches its maximum on 4/14. Even when the magnitudes
786 of the PBAP and FBAP fractions differ on average by a factor of ~ 2 throughout the sampling period, both
787 techniques agree an enhancement in the total biological particles takes place between 4/14 to 4/16. Given
788 the uncertainty of the two methodologies, it is remarkable that there is such agreement between WIBS and
789 FCM results.

790 Among the four meteorological categories, humid and warm days characterize for showing the
791 highest HNA, A type, AB type and ABC type concentrations suggesting that A and AB types may also be
792 related to wet-ejected fungal spores in Metro Atlanta; this possibly explains why the ABC fraction of the
793 total FBAP in 4/7 is not as high as on 4/14 and 4/15 (Figure 3b), and differs with the behavior observed by
794 the HNA population on 4/7. The LNA-AT population does not show a correlation to any specific FBAP
795 type and shows its highest concentrations during dry and cold days. In addition, LNA-AT concentrations are
796 anticorrelated with type B concentrations (Figure S19, correlation coefficient, $r = -0.59$; $R^2 = 0.30$) during
797 dry (both cold and warm) days, when LNA-AT dominates the total PBAP concentration. Given that type B
798 particles have been previously correlated to abiotic particles (e.g. black carbon) in urban environments (Yue

799 et al., 2017), LNA-AT and type B anticorrelation suggests that LNA-AT particles may in fact represent a
800 heterogeneous bioaerosol population. That LNA-AT is not correlated with any FBAP type gives rise to two
801 possibilities: (1) if LNA-AT population is mainly composed of bacteria or agglomerated bacteria, then it is
802 possible that they are detected by multiple FBAP types and is not attributed specifically to one of them; (2)
803 the intrinsic fluorescence of LNA-AT particles is too low and a high fraction of them is abiotic. It is
804 challenging to determine what PBAP types each WIBS FBAP type is mainly detecting. Based on WIBS-
805 4A results in Metro Atlanta, ABC type detects wet-ejected fungal spores, but still unclear what PBAP types
806 are detect by the other FBAP types or if they just capture a high fraction of non-biological particles. FBAP
807 types and WIBS total particles correlations in Figure S17 show all FBAP types are correlated to WIBS total
808 particles, but ABC and AB types show the lowest correlations (type AB: $R^2 = 0.101$; type ABC: $R^2 =$
809 0.1266).

810 Figure 8 shows FCM total PBAP (black line), ABC type (light green), FL1(Channel A; dark green
811 line) and total FBAP (blue line) concentrations, where the FL1 concentration ([FL1]) constitutes the sum
812 of the number concentrations of types A, AB, AC, and ABC ([FL1] = [A] + [AB] + [AC] + [ABC]; Gabey
813 et al., 2011; Healy et al., 2014). Throughout the April-May 2015 sampling events, total PBAP
814 concentrations (1 to 5 μ m) were mainly constrained between the FL1 and ABC type concentrations
815 suggesting FL1 and ABC type represent the upper and lower bound PBAP concentrations in Metro Atlanta,
816 respectively. It also important to highlight that FCM PBAP concentrations are closer to the ABC type
817 concentrations before April 16 when the HNA population dominates, but then after April 16 FCM PBAP
818 concentrations are closer to FL1 concentrations when LNA-AT starts to dominate the total PBAP
819 concentration. In addition, Figure 8 shows that total FBAP (sum of type A, B, C, AB, AC, ABC) exceeds
820 the (corrected) PBAP concentrations in Metro Atlanta.

821

822 **5. Conclusions**

823 In this study we presented the development and testing of an effective FCM protocol to identify and
824 quantify bioaerosol populations. The FCM protocol, designed to constrain any particle accumulation due
825 to cleaning or by fluid supplies, successfully quantified the day-to-day variability of bioaerosols in the
826 Atlanta Metro area. It is the first FCM study to detect well-defined LNA (low nucleic acid) and HNA (high
827 nucleic acid) atmospheric biological populations under different meteorological scenarios. FCM results
828 show dynamic bioaerosol populations in Atlanta leading to a 84.0% of HNA (wet-ejected fungal spores)
829 and 6.1% LNA-AT contribution to the PBAP number (1 to 5 μ m range), respectively, during humid and
830 warm days after rain events. However, LNA-AT dominates warm and cold dry days, constituting 72% of
831 the PBAP number concentration.

832 WIBS-4A and SpinCon II collocated sampling showed that the HNA and ABC type concentrations are
833 well correlated ($R^2=0.40$) and display similar size distributions. We therefore conclude that both
834 instruments detect the same particles, and used empirical collection/detection efficiency factors to correct
835 the FCM size distributions and concentrations in the 1 to 5 μm diameter range. WIBS-4A and FCM results
836 suggest Metro Atlanta PBAP concentrations range between $10^4 - 10^5 \text{ m}^{-3}$ (1 to 5 μm) and they can constitute
837 a substantial fraction of coarse mode particle concentration (WIBS-4A: 43%; FCM: 69%), comparable to
838 the PBAP coarse mode fraction in highly vegetated environments. The FCM LNA-AT population, possibly
839 containing bacterial cells, did not correlate to any FBAP type. The fact that the LNA-AT population is not
840 correlated with a specific FBAP type suggests it may be particularly challenging to use LIF techniques to
841 distinguish bioaerosols with low intrinsic autofluorescence from non-biological particles, especially given
842 the heterogeneities introduced by the large biodiversity of airborne microbes. The possible influence of
843 abiotic particles in the LNA-AT population can also explain the lack of correlation between LNA-AT and
844 FBAP types given that the FCM threshold approach does not ensure total exclusion of abiotic particles. In
845 addition, the unspecific binding of SYTO-13 to abiotic particles cannot be ruled out in the LNA-AT
846 population. FCM comparison between atmospheric and pure culture samples showed lower SYTO-13
847 fluorescence intensities in the atmospheric samples and suggests a degradation in the genetic material of
848 PBAP, possibly caused by the limited nutrients and strong stress prevailing in the atmosphere, which further
849 challenge the ability of LIF to distinguish LNA-AT.

850 In summary, this study have shown for the first time that FCM can effectively identify, quantify and
851 study the daily variability of heterogeneous PBAP populations (e.g. HNA, LNA-AT and pollen) with
852 different genetic material content in an urban environment to the degree of quantitatively correlate FCM
853 HNA to WIBS-4A ABC type number concentrations and better understand wet-ejected fungal spores
854 enhancement after rain events. Furthermore, FCM and WIBS-4A results show bacterial cells detection and
855 quantification still a challenging task for LIF technology as well as for FCM, pointing to the need of
856 concurrent complementary chemometric or molecular biology measurements for unambiguous
857 quantification, given the complexity involved to minimize abiotic interferences, and to the heterogeneity
858 of the atmospheric samples.

859

860 **Acknowledgments**

861 We acknowledge support from a Georgia Power Faculty Scholar chair, a Cullen-Peck Faculty Fellowship,
862 a Dreyfus Foundation Postdoctoral Fellowship in Environmental Chemistry, NASA, a NASA Earth System
863 Science Fellowship (grant no. 80NSSC17K0434). AN acknowledges support from the project PyroTRACH
864 (ERC-2016-COG) funded from H2020-EU.1.1. - Excellent Science - European Research Council (ERC),

865 project ID 726165. We also thank Prof. Rodney Weber for helpful suggestions on the SpinCon II flow
866 calibration.

867

868 **Competing interests**

869 The authors declare no competing interests.

870

871 **Author contributions**

872 AN, AN, KK and MB conceived of the study. AN, NDLR, SW developed the modified biosampler. AN
873 and NDLR developed the FCM analysis and sampling protocol. AN, NDLR carried out measurements, and
874 SW helped support with analysis of the biological samples. LZ, BA provided the WIBS and helped with its
875 setup and initial data analysis procedure. AN, AN worked on the analysis, write codes to interpret the data
876 and developed the analysis protocol to combine the FCM and WIBS analysis outlined here. AN and AN
877 wrote the paper, and all authors contributed significantly with comments and modified text.

878

879 **References**

- 880 Amato, P., Joly, M., Schaupp, C., Attard, E., Möhler, O., Morris, C. E., Brunet, Y., and Delort, A. M.:
881 Survival and ice nucleation activity of bacteria as aerosols in a cloud simulation chamber, *Atmospheric*
882 *Chemistry and Physics Discussions*, 15, 4055-4082, 10.5194/acpd-15-4055-2015, 2015.
- 883 Augustin, S., Hartmann, S., Pummer, B., Grothe, H., Niedermeier, D., Clauss, T., Voigtländer, J.,
884 Tomsche, L., Wex, H., and Stratmann, F.: Immersion freezing of birch pollen washing water,
885 *Atmospheric Chemistry and Physics Discussions*, 12, 32911-32943, 10.5194/acpd-12-32911-2012, 2012.
- 886 Bacsi, A., Choudhury, B. K., Dharajiya, N., Sur, S., and Boldogh, I.: Subpollen particles: carriers of
887 allergenic proteins and oxidases, *J Allergy Clin Immunol*, 118, 844-850, 10.1016/j.jaci.2006.07.006,
888 2006.
- 889 Baillie, L., and Read, T. D.: *Bacillus anthracis*, a bug with attitude!, *Current Opinion in Microbiology*, 4,
890 78-81, [https://doi.org/10.1016/S1369-5274\(00\)00168-5](https://doi.org/10.1016/S1369-5274(00)00168-5), 2001.
- 891 Bauer, H., Claeys, M., Vermeylen, R., Schueller, E., Weinke, G., Berger, A., and Puxbaum, H.: Arabitol
892 and mannitol as tracers for the quantification of airborne fungal spores, *Atmospheric Environment*, 42,
893 588-593, 10.1016/j.atmosenv.2007.10.013, 2008.
- 894 Bauer, H., Schueller, E., Weinke, G., Berger, A., Hitznerberger, R., Marr, I. L., and Puxbaum, H.:
895 Significant contributions of fungal spores to the organic carbon and to the aerosol mass balance of the
896 urban atmospheric aerosol, *Atmospheric Environment*, 42, 5542-5549, 10.1016/j.atmosenv.2008.03.019,
897 2008.
- 898 Bochdansky, A. B., Clouse, M. A., and Herndl, G. J.: Eukaryotic microbes, principally fungi and
899 labyrinthulomycetes, dominate biomass on bathypelagic marine snow, *The Isme Journal*, 11, 362,
900 10.1038/ismej.2016.113, 2016.
- 901 Bouvier, T., Del Giorgio, P. A., and Gasol, J. M.: A comparative study of the cytometric characteristics of
902 high and low nucleic-acid bacterioplankton cells from different aquatic ecosystems, *Environ Microbiol*, 9,
903 2050-2066, 10.1111/j.1462-2920.2007.01321.x, 2007.
- 904 Burrows, S. M., Elbert, W., Lawrence, M. G., and Pöschl, U.: Bacteria in the global atmosphere – Part 1:
905 Review and synthesis of literature data for different ecosystems, *Atmos. Chem. Phys.*, 9, 9263-9280,
906 <https://doi.org/10.5194/acp-9-9263-2009>, 2009.
- 907 Chen, P. S., and Li, C. S.: Bioaerosol characterization by flow cytometry with fluorochrome, *J Environ*
908 *Monit*, 7, 950-959, 10.1039/b505224f, 2005.
- 909 Chi, M.-C., and Li, C.-S.: Fluorochrome in Monitoring Atmospheric Bioaerosols and Correlations with
910 Meteorological Factors and Air Pollutants, *Aerosol Science and Technology*, 41, 672-678,
911 10.1080/02786820701383181, 2007.
- 912 Comas-Riu, J. and Vives-Rego, J. (2002), Cytometric monitoring of growth, sporogenesis and spore cell
913 sorting in *Paenibacillus polymyxa* (formerly *Bacillus polymyxa*). *Journal of Applied Microbiology*, 92:
914 475-481. doi:10.1046/j.1365-2672.2002.01549.x
- 915 Crawford, I., Robinson, N. H., Flynn, M. J., Foot, V. E., Gallagher, M. W., Huffman, J. A., Stanley, W.
916 R., and Kaye, P. H.: Characterization of bioaerosol emissions from a Colorado pine forest: results from

- 917 the BEACHON-RoMBAS experiment, *Atmospheric Chemistry and Physics Discussions*, 14, 2499-2552,
918 10.5194/acpd-14-2499-2014, 2014.
- 919 Darrow, L. A., Hess, J., Rogers, C. A., Tolbert, P. E., Klein, M., and Sarnat, S. E.: Ambient pollen
920 concentrations and emergency department visits for asthma and wheeze, *Journal of Allergy and Clinical*
921 *Immunology*, 130, 630-638.e634, <https://doi.org/10.1016/j.jaci.2012.06.020>, 2012.
- 922 DeLeon-Rodriguez, N., Terry L. Lathem, Luis M. Rodriguez-R, James M. Barazesh, Bruce E. Anderson,
923 Andreas J. Beyersdorf, Luke D. Ziemba, Michael Bergin, Athanasios Nenes, and Konstantinos T.
924 Konstantinidis.: Microbiome of the upper troposphere: Species composition and prevalence, effects of
925 tropical storms, and atmospheric implications, *Proceedings of the National Academy of Sciences* 110,
926 2575-2580, 2013.
- 927 DeLeon-Rodriguez, N.: Microbes in the atmosphere: prevalence, species composition, and relevance to
928 cloud formation School of Biology Georgia Institute of Technology, 129 pp.,
929 (<http://hdl.handle.net/1853/55517>), 2015.
- 930 Delort, A.-M., and Amato, P.: *Microbiology of aerosols*, pp.167-168, 2018.
- 931 Després, V. R., Alex Huffman, J., Burrows, S. M., Hoose, C., Safatov, A. S., Buryak, G., Fröhlich-
932 Nowoisky, J., Elbert, W., Andreae, M. O., Pöschl, U., and Jaenicke, R.: Primary biological aerosol
933 particles in the atmosphere: a review, *Tellus B*, 64, 10.3402/tellusb.v64i0.15598, 2012.
- 934 Díaz, M., Herrero, M., García, L. A., and Quirós, C.: Application of flow cytometry to industrial
935 microbial bioprocesses, *Biochemical Engineering Journal*, 48, 385-407,
936 <https://doi.org/10.1016/j.bej.2009.07.013>, 2010.
- 937 Eckenrode, H. M., Jen, S.-H., Han, J., Yeh, A.-G., and Dai, H.-L.: Adsorption of a Cationic Dye Molecule
938 on Polystyrene Microspheres in Colloids: Effect of Surface Charge and Composition Probed by Second
939 Harmonic Generation, *The Journal of Physical Chemistry B*, 109, 4646-4653, 10.1021/jp045610q, 2005.
- 940 Elbert, W., Taylor, P. E., Andreae, M. O., & Pöschl, U.: Contribution of fungi to primary biogenic
941 aerosols in the atmosphere: wet and dry discharged spores, carbohydrates, and inorganic ions.,
942 *Atmospheric Chemistry and Physics*, 7, 4569-4588, 2007.
- 943 Fröhlich-Nowoisky, J., Kampf, C. J., Weber, B., Huffman, J. A., Pöhlker, C., Andreae, M. O., Lang-
944 Yona, N., Burrows, S. M., Gunthe, S. S., Elbert, W., Su, H., Hoor, P., Thines, E., Hoffmann, T., Després,
945 V. R., and Pöschl, U.: Bioaerosols in the Earth system: Climate, health, and ecosystem interactions,
946 *Atmospheric Research*, 182, 346-376, <http://dx.doi.org/10.1016/j.atmosres.2016.07.018>, 2016.
- 947 Gabey, A. M., Gallagher, M. W., Whitehead, J., Dorsey, J. R., Kaye, P. H., and Stanley, W. R.:
948 Measurements and comparison of primary biological aerosol above and below a tropical forest canopy
949 using a dual channel fluorescence spectrometer, *Atmospheric Chemistry and Physics*, 10, 4453-4466,
950 10.5194/acp-10-4453-2010, 2010.
- 951 Gabey, A. M., Stanley, W. R., Gallagher, M. W., and Kaye, P. H.: The fluorescence properties of aerosol
952 larger than 0.8 μm in urban and tropical rainforest locations, *Atmospheric Chemistry and Physics*, 11,
953 5491-5504, 10.5194/acp-11-5491-2011, 2011.
- 954 Gosselin, M. I., Rathnayake, C. M., Crawford, I., Pöhlker, C., Fröhlich-Nowoisky, J., Schmer, B.,
955 Després, V. R., Engling, G., Gallagher, M., Stone, E., Pöschl, U., and Huffman, J. A.: Fluorescent

956 bioaerosol particle, molecular tracer, and fungal spore concentrations during dry and rainy periods in a
957 semi-arid forest, *Atmos. Chem. Phys.*, 16, 15165-15184, 10.5194/acp-16-15165-2016, 2016.

958 Goudie, A. S.: Desert dust and human health disorders, *Environment International*, 63, 101-113,
959 <http://dx.doi.org/10.1016/j.envint.2013.10.011>, 2014.

960 Griffin, D. W., Kellogg, C. A., Garrison, V. H., Lisle, J. T., Borden, T. C., and Shinn, E. A.: Atmospheric
961 microbiology in the northern Caribbean during African dust events, *Aerobiologia*, 19, 143-157,
962 10.1023/B:AERO.0000006530.32845.8d, 2003.

963 Grote, M., Valenta, R., and Reichelt, R.: Abortive pollen germination: A mechanism of allergen release in
964 birch, alder, and hazel revealed by immunogold electron microscopy, *J. Allergy Clin. Immun.*, 111, 1017–
965 1023, doi:10.1067/mai.2003.1452, 2003.

966 Guarín, F. A., Abril, M. A. Q., Alvarez, A., and Fonnegra, R.: Atmospheric pollen and spore content in
967 the urban area of the city of Medellin, Colombia, *Hoehnea*, 42, 9-19, 2015.

968 Guindulain, T., J. Comas, and J. Vives-Rego: Use of nucleic acid dyes SYTO-13, TOTO-1, and YOYO-1
969 in the study of *Escherichia coli* and marine prokaryotic populations by flow cytometry, *Applied and*
970 *environmental microbiology*, 63, 4608 - 4611, 1997.

971 Harrison, R. M., Jones, A. M., Biggins, P. D. E., Pomeroy, N., Cox, C. S., Kidd, S. P., Hobman, J. L.,
972 Brown, N. L., and Beswick, A.: Climate factors influencing bacterial count in background air samples,
973 *International Journal of Biometeorology*, 49, 167-178, 10.1007/s00484-004-0225-3, 2005.

974 Healy, D. A., Huffman, J. A., O'Connor, D. J., Pöhlker, C., Pöschl, U., and Sodeau, J. R.: Ambient
975 measurements of biological aerosol particles near Killarney, Ireland: a comparison between real-time
976 fluorescence and microscopy techniques, *Atmos. Chem. Phys.*, 14, 8055-8069, 10.5194/acp-14-8055-
977 2014, 2014.

978 Healy, D. A., O'Connor, D. J., and Sodeau, J. R.: Measurement of the particle counting efficiency of the
979 “Waveband Integrated Bioaerosol Sensor” model number 4 (WIBS-4), *Journal of Aerosol Science*, 47,
980 94-99, <http://dx.doi.org/10.1016/j.jaerosci.2012.01.003>, 2012.

981 Hernandez, M., Perring, A. E., McCabe, K., Kok, G., Granger, G., and Baumgardner, D.: Chamber
982 catalogues of optical and fluorescent signatures distinguish bioaerosol classes, *Atmos. Meas. Tech.*, 9,
983 3283-3292, <https://doi.org/10.5194/amt-9-3283-2016>, 2016.

984 Hill, S. C., Mayo, M. W., and Chang, R. K.: Fluorescence of bacteria, pollens, and naturally occurring
985 airborne particles: excitation/emission spectra, Army Research Lab Adelphi Md Computational And
986 Information Sciences Directorate, 2009.

987 Hoose, C., Kristjánsson, J. E., and Burrows, S. M.: How important is biological ice nucleation in clouds
988 on a global scale?, *Environmental Research Letters*, 5, 024009, 2010.

989 Hoose, C., and Möhler, O.: Heterogeneous ice nucleation on atmospheric aerosols: a review of results
990 from laboratory experiments, *Atmos. Chem. Phys.*, 12, 9817-9854, 10.5194/acp-12-9817-2012, 2012.

991 Huffman, J. A., B. Treutlein, and U. Pöschl: Fluorescent biological aerosol particle concentrations and
992 size distributions measured with an Ultraviolet Aerodynamic Particle Sizer (UV-APS) in Central Europe,
993 *Atmospheric Chemistry and Physics*, 10, 3215-3233, 2010.

- 994 Huffman, J. A., Prenni, A. J., DeMott, P. J., Pöhlker, C., Mason, R. H., Robinson, N. H., Fröhlich-
 995 Nowoisky, J., Tobo, Y., Després, V. R., Garcia, E., Gochis, D. J., Harris, E., Müller-Germann, I., Ruzene,
 996 C., Schmer, B., Sinha, B., Day, D. A., Andreae, M. O., Jimenez, J. L., Gallagher, M., Kreidenweis, S. M.,
 997 Bertram, A. K., and Pöschl, U.: High concentrations of biological aerosol particles and ice nuclei during
 998 and after rain, *Atmospheric Chemistry and Physics*, 13, 6151-6164, 10.5194/acp-13-6151-2013, 2013.
- 999 Ingold, C. T.: Fungal spores. Their liberation and dispersal, Oxford, Clarendon Press., 302 pp. pp., 1971.
- 1000 Joly, M., Amato, P., Sancelme, M., Vinatier, V., Abrantes, M., Deguillaume, L., and Delort, A.-M.:
 1001 Survival of microbial isolates from clouds toward simulated atmospheric stress factors, *Atmospheric*
 1002 *Environment*, 117, 92-98, <https://doi.org/10.1016/j.atmosenv.2015.07.009>, 2015.
- 1003 Joung, Y. S., and Buie, C. R.: Aerosol generation by raindrop impact on soil, 6, 6083,
 1004 10.1038/ncomms7083, <https://www.nature.com/articles/ncomms7083#supplementary-information>, 2015.
- 1005 Kesavan, J., and Sagripanti, J. L.: Evaluation criteria for bioaerosol samplers, *Environ Sci Process*
 1006 *Impacts*, 17, 638-645, 10.1039/c4em00510d, 2015.
- 1007 Lange, J. L. T., P S and Lynch, N: Application of flow cytometry and fluorescent in situ hybridization for
 1008 assessment of exposures to airborne bacteria *Appl. Environ. Microbiol.* , 63, 1557-1563, 1997.
- 1009 Lebaron, P., Servais, P., Agogue, H., Courties, C., and Joux, F.: Does the high nucleic acid content of
 1010 individual bacterial cells allow us to discriminate between active cells and inactive cells in aquatic
 1011 systems?, *Appl Environ Microbiol*, 67, 1775-1782, 10.1128/AEM.67.4.1775-1782.2001, 2001.
- 1012 Li, D.-W., and Bryce Kendrick: A year-round study on functional relationships of airborne fungi with
 1013 meteorological factors, *International Journal of Biometeorology* 39, 74-80, 1995.
- 1014 Liang, L., Engling, G., Cheng, Y., Duan, F., Du, Z., and He, K.: Rapid detection and quantification of
 1015 fungal spores in the urban atmosphere by flow cytometry, *Journal of Aerosol Science*, 66, 179-186,
 1016 10.1016/j.jaerosci.2013.08.013, 2013.
- 1017 Lin, H., Gomez, I., and Meredith, J. C.: Pollenkit Wetting Mechanism Enables Species-Specific Tunable
 1018 Pollen Adhesion, *Langmuir*, 29, 3012-3023, 10.1021/la305144z, 2013.
- 1019 Longo, A. F., Ingall, E. D., Diaz, J. M., Oakes, M., King, L. E., Nenes, A., Mihalopoulos, N., Violaki, K.,
 1020 Avila, A., Benitez-Nelson, C. R., Brandes, J., McNulty, I., and Vine, D. J.: P-NEXFS analysis of aerosol
 1021 phosphorus delivered to the Mediterranean Sea, *Geophysical Research Letters*, 41, 4043-4049,
 1022 10.1002/2014GL060555, 2014.
- 1023 Monier, J. M., and Lindow, S. E.: *Pseudomonas syringae* Responds to the Environment on Leaves by Cell
 1024 Size Reduction, *Phytopathology*, 93, 1209-1216, 10.1094/PHYTO.2003.93.10.1209, 2003.
- 1025 Morris, C. E., Conen, F., Alex Huffman, J., Phillips, V., Poschl, U., and Sands, D. C.: Bioprecipitation: a
 1026 feedback cycle linking earth history, ecosystem dynamics and land use through biological ice nucleators
 1027 in the atmosphere, *Glob Chang Biol*, 20, 341-351, 10.1111/gcb.12447, 2014.
- 1028 Muller, S., and Nebe-von-Caron, G.: Functional single-cell analyses: flow cytometry and cell sorting of
 1029 microbial populations and communities, *FEMS Microbiol Rev*, 34, 554-587, 10.1111/j.1574-
 1030 6976.2010.00214.x, 2010.

- 1031 Myriokefalitakis, S., Nenes, A., Baker, A. R., Mihalopoulos, N., and Kanakidou, M.: Bioavailable
1032 atmospheric phosphorous supply to the global ocean: a 3-D global modeling study, *Biogeosciences*, 13,
1033 6519-6543, 10.5194/bg-13-6519-2016, 2016.
- 1034 Nir, R., Yisraeli, Y., Lamed, R., & Sahar, E.: Flow cytometry sorting of viable bacteria and yeasts
1035 according to beta-galactosidase activity, *Applied and environmental microbiology*, 56, 3861-3866, 1990.
- 1036 Oliveira, M., Ribeiro, H., Delgado, J. L., and Abreu, I.: The effects of meteorological factors on airborne
1037 fungal spore concentration in two areas differing in urbanisation level, *Int J Biometeorol*, 53, 61-73,
1038 10.1007/s00484-008-0191-2, 2009.
- 1039
- 1040 Ortiz-Martínez, Mario G., Rosa I. Rodríguez-Cotto, Mónica A. Ortiz-Rivera, Cedric W. Pluguez-Turull,
1041 and Braulio D. Jiménez-Vélez. Linking endotoxins, African dust PM10 and asthma in an urban and rural
1042 environment of Puerto Rico. *Mediators of inflammation* 2015.
- 1043 Pan, Y.-L., Santarpia, J. L., Ratnesar-Shumate, S., Corson, E., Eshbaugh, J., Hill, S. C., Williamson, C. C.,
1044 Coleman, M., Bare, C., and Kinahan, S.: Effects of ozone and relative humidity on fluorescence spectra of
1045 octapeptide bioaerosol particles, *Journal of Quantitative Spectroscopy and Radiative Transfer*, 133, 538-
1046 550, <https://doi.org/10.1016/j.jqsrt.2013.09.017>, 2014.
- 1047 Perring, A. E., et al. (2015), Airborne observations of regional variation in fluorescent aerosol across the
1048 United States, *J. Geophys. Res. Atmos.*, 120, 1153–1170, doi:10.1002/2014JD022495.
- 1049 Pöhlker, C., Huffman, J. A., Förster, J. D., and Pöschl, U.: Autofluorescence of atmospheric bioaerosols:
1050 spectral fingerprints and taxonomic trends of pollen, *Atmospheric Measurement Techniques*, 6, 3369-
1051 3392, 10.5194/amt-6-3369-2013, 2013.
- 1052 Pöhlker, C., Huffman, J. A., and Pöschl, U.: Autofluorescence of atmospheric bioaerosols – fluorescent
1053 biomolecules and potential interferences, *Atmospheric Measurement Techniques*, 5, 37-71, 10.5194/amt-
1054 5-37-2012, 2012.
- 1055 Pöschl, U.: Atmospheric Aerosols: Composition, Transformation, Climate and Health Effects,
1056 *Angewandte Chemie International Edition*, 44, 7520-7540, 10.1002/anie.200501122, 2005.
- 1057 Robinson, N. H., Allan, J. D., Huffman, J. A., Kaye, P. H., Foot, V. E., and Gallagher, M.: Cluster
1058 analysis of WBS single-particle bioaerosol data, *Atmos. Meas. Tech.*, 6, 337-347,
1059 <https://doi.org/10.5194/amt-6-337-2013>, 2013.
- 1060 Rödiger, S., Ruhland, M., Schmidt, C., Schröder, C., Grossmann, K., Böhm, A., Nitschke, J., Berger, I.,
1061 Schimke, I., and Schierack, P.: Fluorescence Dye Adsorption Assay to Quantify Carboxyl Groups on the
1062 Surface of Poly(methyl methacrylate) Microbeads, *Analytical Chemistry*, 83, 3379-3385,
1063 10.1021/ac103277s, 2011.
- 1064 S.-L. Von der Weiden, F. D., and S. Borrmann: Particle Loss Calculator - a new software tool for the
1065 assessment of the performance of aerosol inlet systems, *Atmospheric Measurement Techniques*, 2, 479-
1066 494, 2009.
- 1067 Saari, S., Reponen, T., and Keskinen, J.: Performance of Two Fluorescence-Based Real-Time Bioaerosol
1068 Detectors: BioScout vs. UVAPS, *Aerosol Science and Technology*, 48, 371-378,
1069 10.1080/02786826.2013.877579, 2014.

- 1070 Šantl-Temkiv, T., Amato, P., Gosewinkel, U., Thyrhaug, R., Charton, A., Chicot, B., Finster, K., Bratbak,
1071 G., and Löndahl, J.: High-Flow-Rate Impinger for the Study of Concentration, Viability, Metabolic
1072 Activity, and Ice-Nucleation Activity of Airborne Bacteria, *Environmental Science & Technology*, 51,
1073 11224-11234, 10.1021/acs.est.7b01480, 2017.
- 1074 Savage, N. J., Krentz, C. E., Könemann, T., Han, T. T., Mainelis, G., Pöhlker, C., and Huffman, J. A.:
1075 Systematic characterization and fluorescence threshold strategies for the wideband integrated bioaerosol
1076 sensor (WIBS) using size-resolved biological and interfering particles, *Atmospheric Measurement
1077 Techniques*, 10, 4279-4302, 10.5194/amt-10-4279-2017, 2017.
- 1078 Standaert-Vitse, A., Aliouat-Denis, C.-M., Martinez, A., Khalife, S., Pottier, M., Gantois, N., Dei-Cas, E.,
1079 and Aliouat, E. M.: SYTO-13, a Viability Marker as a New Tool to Monitor In Vitro Pharmacodynamic
1080 Parameters of Anti-Pneumocystis Drugs, *PLoS One*, 10, e0130358-e0130358,
1081 10.1371/journal.pone.0130358, 2015.
- 1082 Sullivan, S. C., Hoose, C., Kiselev, A., Leisner, T., and Nenes, A.: Initiation of secondary ice production
1083 in clouds, *Atmos. Chem. Phys. Discuss.*, 2017, 1-22, 10.5194/acp-2017-387, 2017.
- 1084 Taylor, P. E., Jacobson, K. W., House, J. M., and Glovsky, M. M.: Links between pollen, atopy and the
1085 asthma epidemic, *Int Arch Allergy Immunol*, 144, 162-170, 10.1159/000103230, 2007.
- 1086 Toprak, E., and Schnaiter, M.: Fluorescent biological aerosol particles measured with the Waveband
1087 Integrated Bioaerosol Sensor WIBS-4: laboratory tests combined with a one year field study,
1088 *Atmospheric Chemistry and Physics*, 13, 225-243, 10.5194/acp-13-225-2013, 2013.
- 1089 Van Dilla, M. A., Langlois, R. G., Pinkel, D., Yajko, D., & Hadley, W. K.: Bacterial characterization by
1090 flow cytometry., *Science*, 220, 620-622, 1983.
- 1091 Wang, Y., Hammes, F., De Roy, K., Verstraete, W., and Boon, N.: Past, present and future applications of
1092 flow cytometry in aquatic microbiology, *Trends Biotechnol*, 28, 416-424, 10.1016/j.tibtech.2010.04.006,
1093 2010.
- 1094 Wu, Y.-H., Chan, C.-C., Rao, C. Y., Lee, C.-T., Hsu, H.-H., Chiu, Y.-H., and Chao, H. J.: Characteristics,
1095 determinants, and spatial variations of ambient fungal levels in the subtropical Taipei metropolis,
1096 *Atmospheric Environment*, 41, 2500-2509, 10.1016/j.atmosenv.2006.11.035, 2007.
- 1097 Yu, X., Wang, Z., Zhang, M., Kuhn, U., Xie, Z., Cheng, Y., Pöschl, U., and Su, H.: Ambient
1098 measurement of fluorescent aerosol particles with a WIBS in the
- 1099 Yangtze River Delta of China: potential impacts of combustion-related aerosol particles, *Atmospheric
1100 Chemistry and Physics*, 16, 11337-11348, 10.5194/acp-16-11337-2016, 2016.
- 1101 Yue, S., Ren, H., Fan, S., Sun, Y., Wang, Z., and Fu, P.: Springtime precipitation effects on the
1102 abundance of fluorescent biological aerosol particles and HULIS in Beijing, *Sci Rep*, 6, 29618,
1103 10.1038/srep29618, 2016.
- 1104 Yue, S., Ren, H., Fan, S., Wei, L., Zhao, J., Bao, M., Hou, S., Zhan, J., Zhao, W., Ren, L., Kang, M., Li,
1105 L., Zhang, Y., Sun, Y., Wang, Z., and Fu, P.: High Abundance of Fluorescent Biological Aerosol
1106 Particles in Winter in Beijing, China, *ACS Earth and Space Chemistry*, 1, 493-502,
1107 10.1021/acsearthspacechem.7b00062, 2017.

- 1108 Zhen, H., Han, T., Fennell, D. E., and Mainelis, G.: Release of free DNA by membrane-impaired bacterial
1109 aerosols due to aerosolization and air sampling, *Appl Environ Microbiol*, 79, 7780-7789,
1110 10.1128/AEM.02859-13, 2013.
- 1111 Ziemba, L. D., Beyersdorf, A. J., Chen, G., Corr, C. A., Crumeyrolle, S. N., Diskin, G., Hudgins, C.,
1112 Martin, R., Mikoviny, T., Moore, R., Shook, M., Thornhill, K. L., Winstead, E. L., Wisthaler, A., and
1113 Anderson, B. E.: Airborne observations of bioaerosol over the Southeast United States using a Wideband
1114 Integrated Bioaerosol Sensor, *Journal of Geophysical Research: Atmospheres*, 121, 8506-8524,
1115 10.1002/2015JD024669, 2016.
- 1116

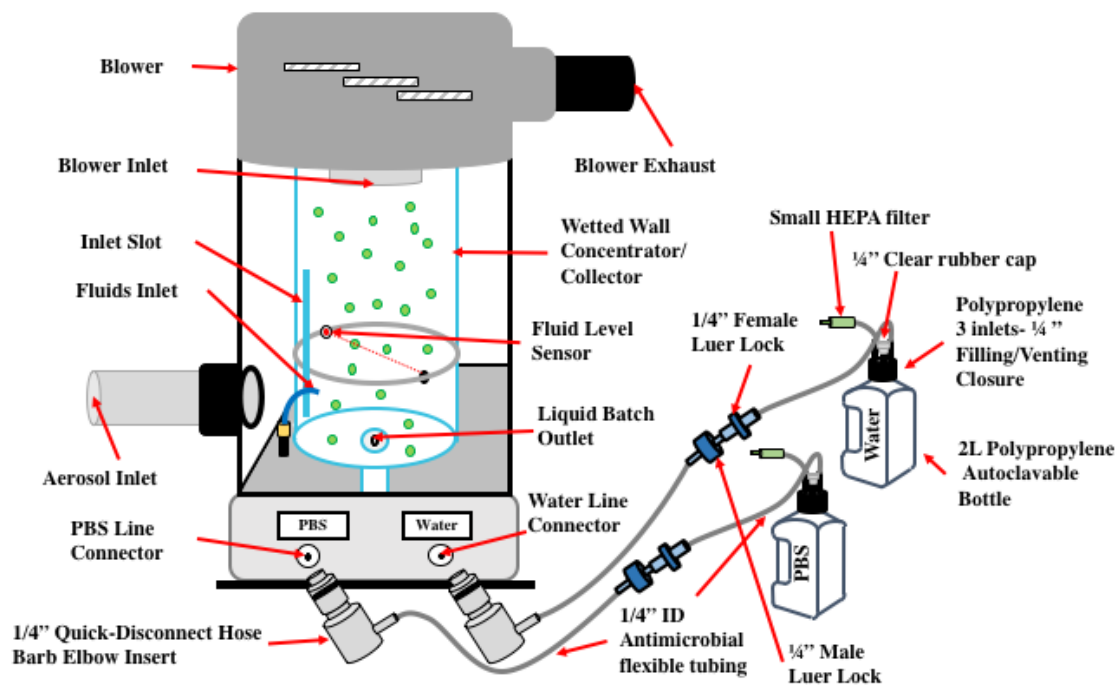
1 **Table 1:** Summary of the SpinCon II sampling events, the 24 h. averaged RH, ambient temperature, the
 2 assigned meteorological category (using Section 4.4 definitions) and the corrected FCM-derived PBAP
 3 number concentration (1 to 5 μm) for each sample collected during this study.

4
5

Date (starting – ending time)	RH (%)	Temperature (°C)	Meteorological Category	PBAP Concentration (m^{-3}) 1 to 5μm diameter range
4/7/15 (11:17 - 15:17) *	70.9	21.4	Humid, Warm	9.282×10^4
4/8/15 (11:10 - 15:10)	53.6	24.9	Dry, Warm	5.203×10^5
4/9/15 (11:15 - 15:15)	53.8	25.3	Dry, Warm	1.254×10^5
4/14/15 (11:30 - 15:30) *	76.8	22.5	Humid, Warm	8.253×10^4
4/15/15 (11:40 - 15:40) *	83.6	18.9	Humid, Warm	1.234×10^5
4/16/15 (10:55 - 14:55)	86.3	12.5	Humid, Cold	3.399×10^5
4/21/15 (13:15 - 17:15)	43.2	16.6	Dry, Cold	4.741×10^5
4/22/15 (11:25 - 15:25)	41.2	19.0	Dry, Warm	3.351×10^5
4/23/15 (11:35 - 15:35)	48.1	16.8	Dry, Cold	1.708×10^6
4/28/15 (12:25 - 16:25)	45.3	17.0	Dry, Cold	4.899×10^5
4/29/15 (11:55 - 15:55) #	79.4	14.2	Humid, Cold	4.591×10^5
4/30/15 (12:10 - 16:10)	57.3	17.4	Dry, Cold	9.603×10^5
5/13/15 (10:50 - 14:50)	40.1	23.5	Dry, Warm	3.680×10^5
5/14/15 (11:50 - 15:50)	52.3	23.0	Dry, Warm	4.851×10^5
5/15/15 (10:19 - 14:19)	64.4	23.1	Dry, Warm	1.656×10^6

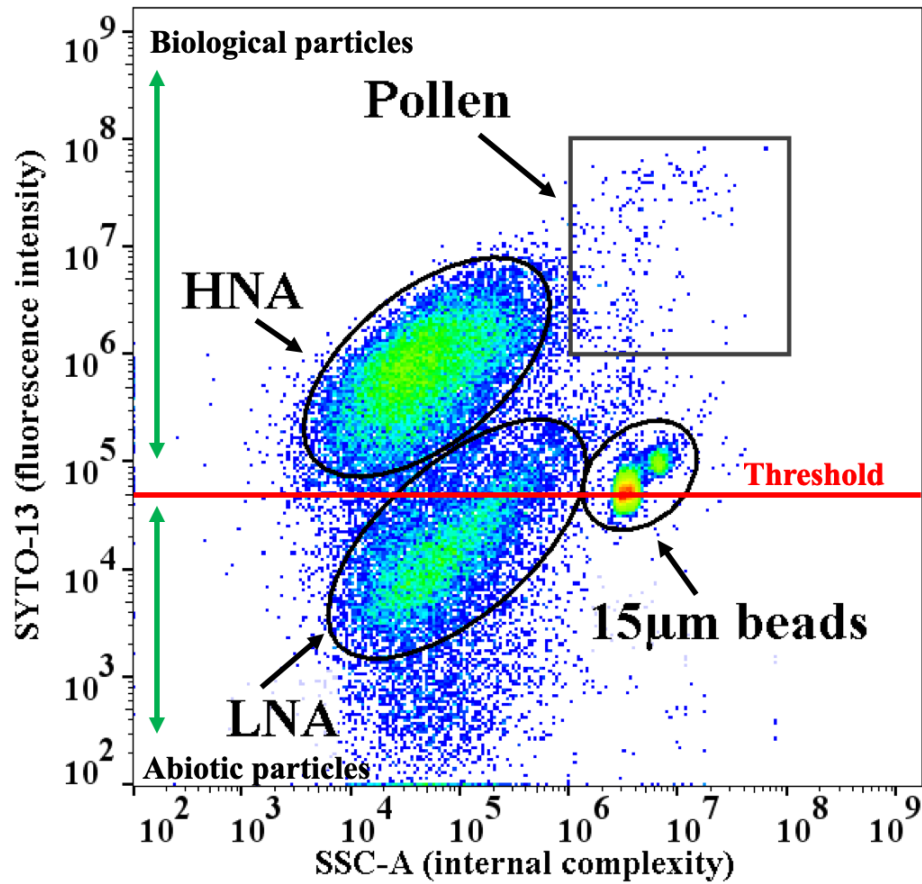
6 * Sampling occurred post-rain event.
 7 # Sampling occurred during a rain event.

8



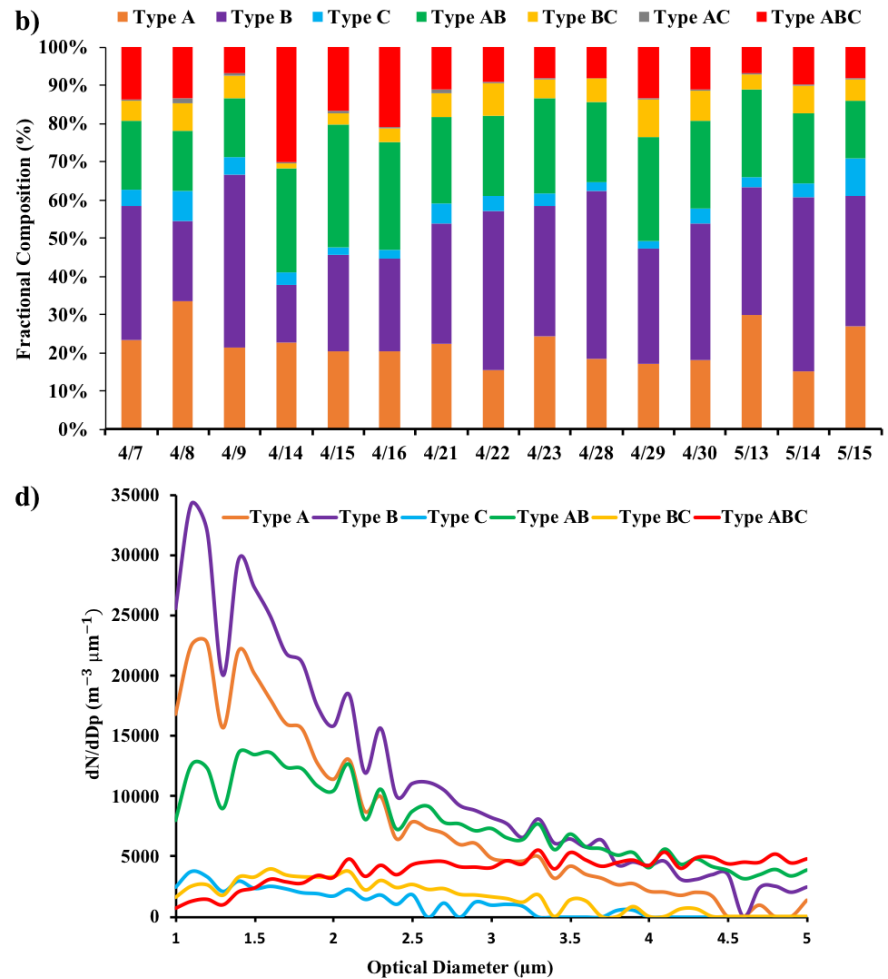
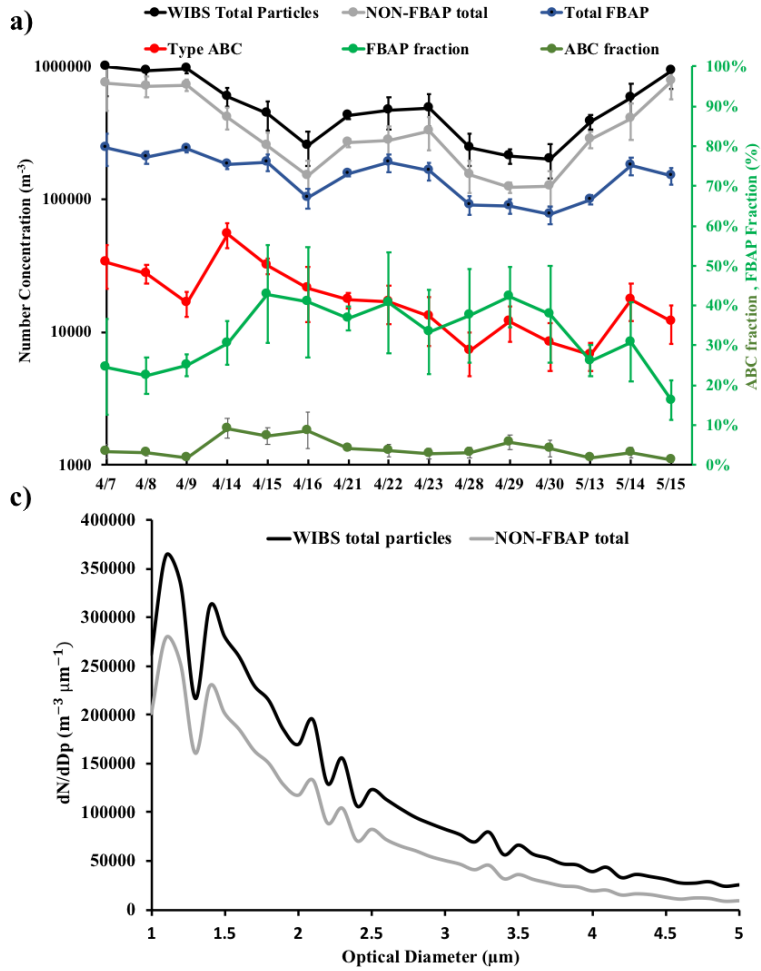
9
10
11
12

Figure 1: SpinCon II sampling setup including modified fluid supply system with anti-microbial tubing and 2L Autoclavable bottles.



13
 14
 15
 16
 17
 18
 19
 20
 21

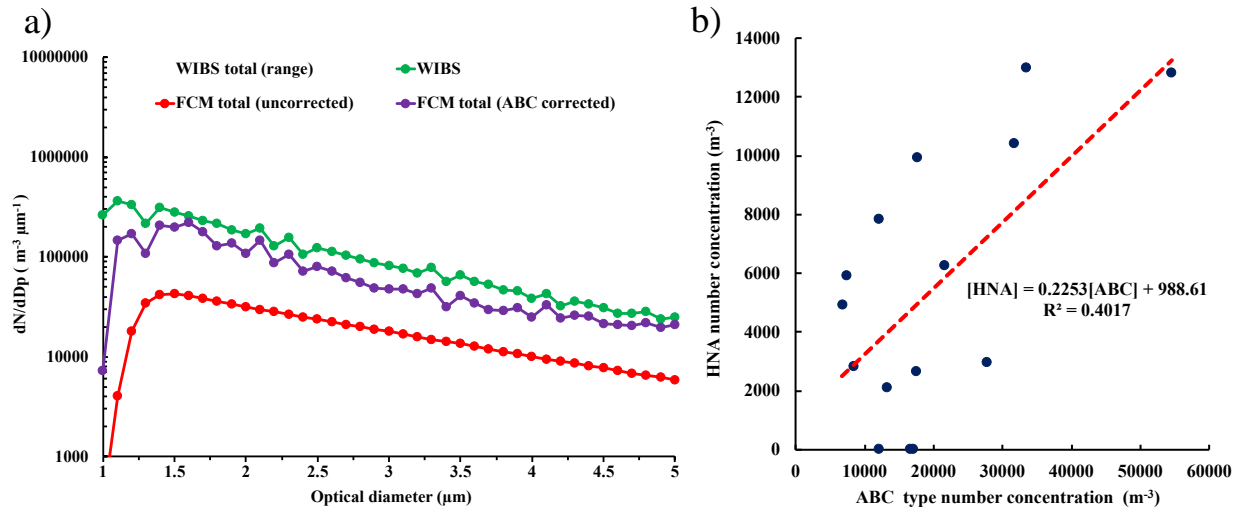
Figure 2: FL1-A vs. SSC-A plot used to identify populations in the April 14, 2015 sample including: the 42k threshold line in red and, abiotic particles (below threshold) and biological particles (above threshold) designated regions. In the density plot green and red zones denote the most populated regions. FL1-A in the y-axis shows the fluorescence intensity of each particle in the plot stained with SYTO-13 and SSC-A in the x-axis measures 90° light scattering, related to the internal complexity of the particles. The fraction of the LNA population above the threshold line is referred as the “LNA-AT” population.



22

23 **Figure 3:** WIBS-4A 4hr (SpinCon II sampling time) averaged results of WIBS total particle, NON-FBAP, total FBAP and type ABC concentrations in the left Y-axis and ABC and FBAP fraction in the right Y-axis for each SpinCon II sampling event in (a); 4hr averaged FBAP types number
 24 concentration fractional composition for each SpinCon II sampling event in (b); 1to5μm WIBS total particles and NON-FBAP size distributions in
 25 (c) and 1to5μm size distributions for all FBAP types, except AC type in (d). AC type showed low statistics and constituted less than 1% of the total
 26 FBAP (not shown). Size distributions in (c) and (d) have been averaged over the 15 SpinCon II sampling events and constitute the overall size
 27 distributions during rooftop sampling events.
 28

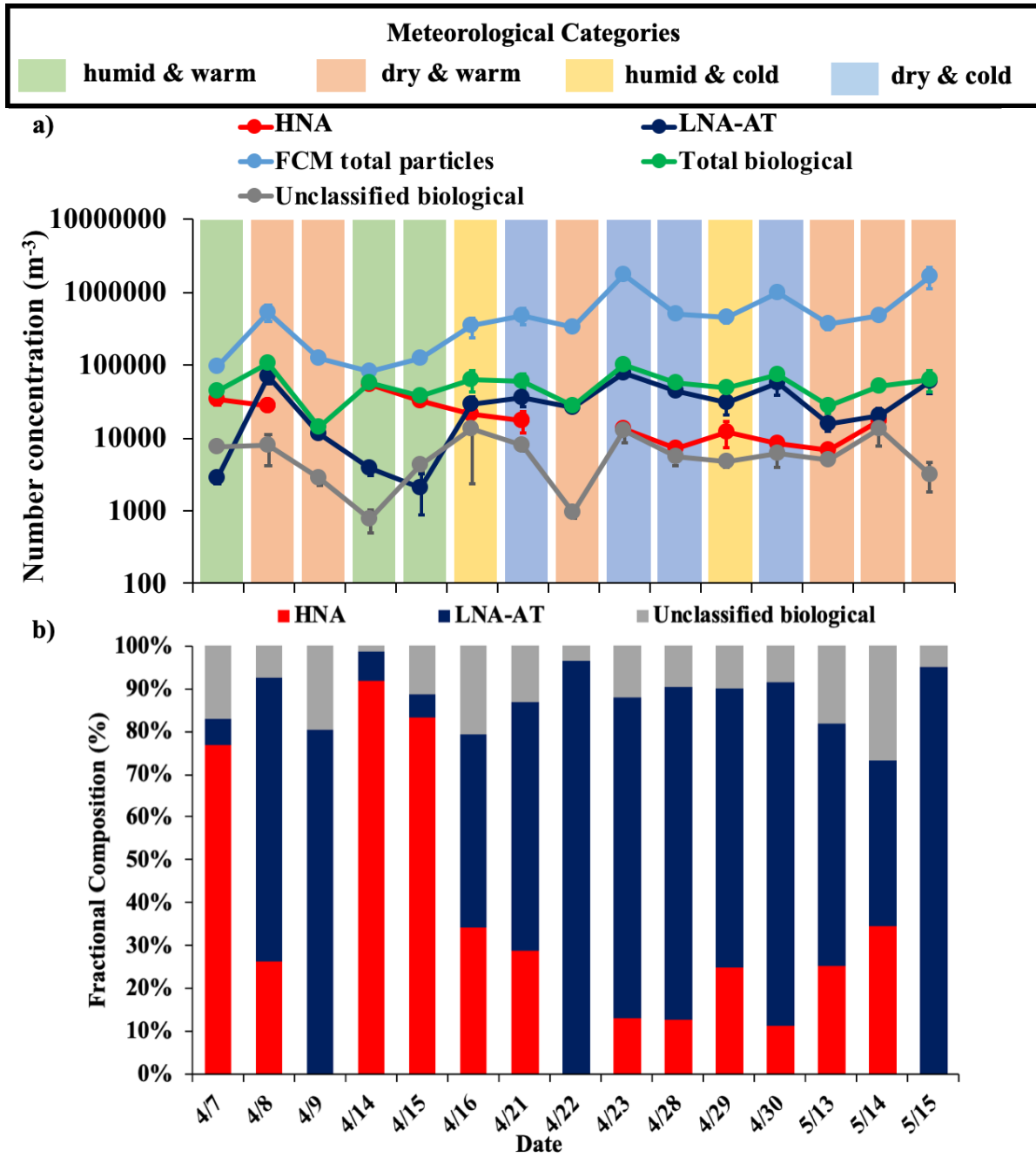
29
30



31
32
33
34
35
36
37
38

Figure 4: WIBS-4A, FCM uncorrected and FCM (ABC corrected) total particle concentration (1 to 5 μ m) average size distributions (geometrically averaged over the 15 SpinCon II sampling events) including WIBS range (\pm geometric standard deviation factor) in (a); and HNA and ABC type concentration correlation in the 1 to 5 μ m range in (b) including its linear correlation in red.

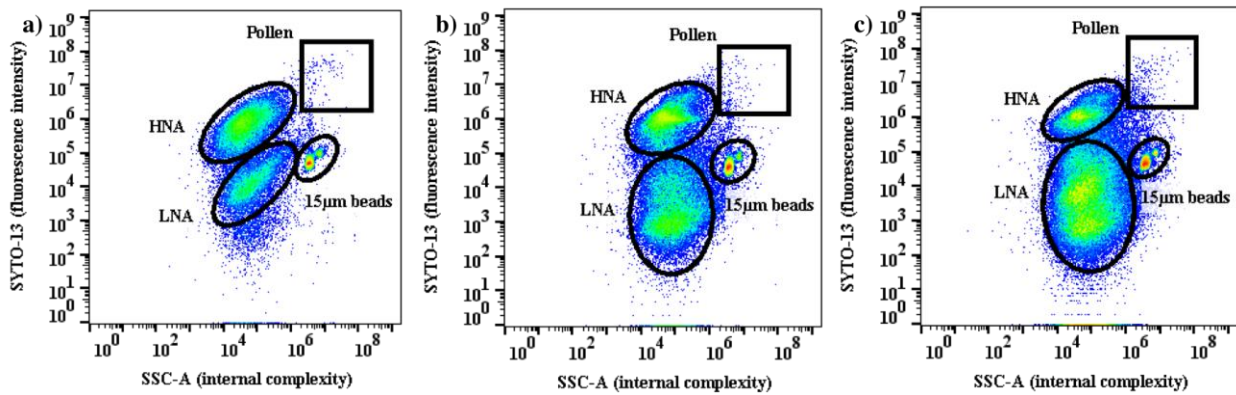
39
40



41
42
43
44
45
46
47
48
49
50

Figure 5: FCM total particle, HNA, LNA-AT and total PBAP number concentrations in the 1 to 5µm range highlighting the prevailing meteorological category during each sampling event in (a); HNA and LNA-AT number concentration fractional compositions for each sampling event in (b).

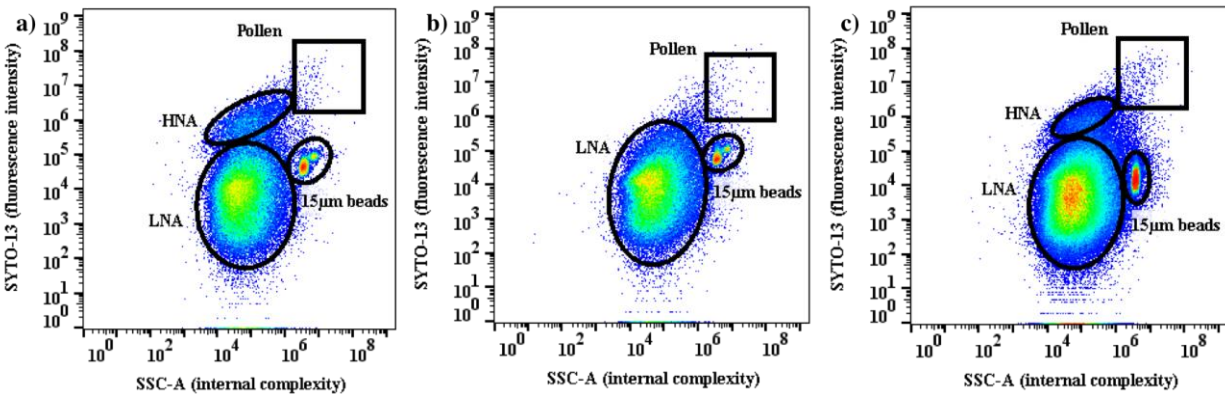
51
52
53



54
55

56 **Figure 6:** FL1-A vs. SSC-A FSC plots for (a) April 14, (b) April 15, and, (c) April 16. This period was
57 characterized by a transition from humid & warm to humid & cold conditions (diurnal average RH=77%,
58 T=22.5 °C on 4/14; RH=84%, T=18.9 °C on 4/15, and RH= 86%, T= 12.5 °C on 4/16). The FCM plots
59 during this transition period show a decrease of fungal population and an increase of the LNA population.
60 In each population, warmer colors represent higher particle concentrations.

61
62
63

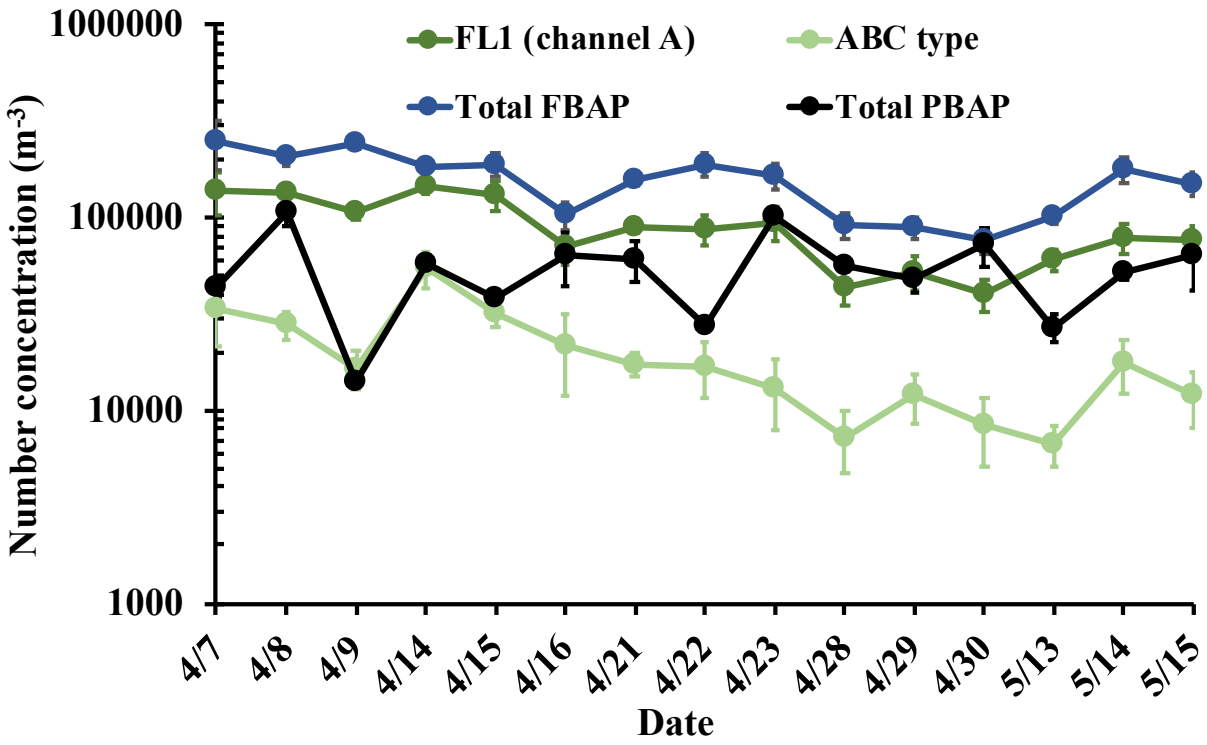


64
65
66

67 **Figure 7:** Similar to Figure 6, but for (a) April 21, (b) April 22, (c) April 23, which was characterized by
68 dry and variability in temperature (diurnal average RH=43%, T=16.6 °C on 4/21; RH=41%, T=19.0 °C on
69 4/22, and, RH= 48%, T= 16.8 °C on 4/23). Note the disappearance of the fungal spore population on the
70 warmest day (4/22).

71
72
73
74
75
76

77
78



79
80
81
82
83
84
85
86
87
88
89
90
91

Figure 8: WIBS-4A total FBAP, FL1 and ABC type, and FCM total particle number concentrations in the 1 to 5 μ m range for each sampling event from April 7 to May 15, 2015.